J. Fluid Mech. (1992), *vol.* 243, *pp.* 393–441
Printed in Great Britain

The natural and forced formation of spot-like 'vortex dislocations' in the transition of a wake

By C. H. K. WILLIAMSON
Mechanical and Aerospace Engineering, Upson Hall, Cornell University, Ithaca, NY 14853, USA

(Received 29 August 1991 and in revised form 14 February 1992)

The three-dimensional transition of the flow behind a bluff body is studied, with an emphasis placed on the evolution of large-scale structures in the wake. It has previously been found that there are two fundamental modes of three-dimensional vortex shedding in the wake of a circular cylinder (each mode being dependent on the range of Reynolds number), with a spanwise lengthscale of the same order as the primary streamwise wavelength of the vortex street. However, it is shown in the present study that the wake transition also involves the appearance of large-scale spot-like 'vortex dislocations', that grow downstream to a size of the order of 10–20 primary wavelengths. Vortex dislocations are generated between spanwise vortex-shedding cells of different frequency. The presence of these dislocations explains the large intermittent velocity irregularities that were originally found by Roshko (1954) and later by Bloor (1964) to characterize transition. The presence of these vortex dislocations in wake transition is largely responsible for the break-up to turbulence of the wake as it travels downstream.

In order to study their evolution in detail, dislocations have been (passively) forced to occur at a local spanwise position with the use of a small ring disturbance. It is found that 'two-sided' dislocations are stable in a symmetric in-phase configuration, and that they induce quasi-periodic velocity spectra and (beat) dislocation-frequency oscillations in the near wake. Intrinsic to these dislocations is a mechanism by which they spread rapidly in the spanwise direction, involving helical twisting of the vortices and axial core flows. This is felt to be a fundamental mechanism by which vortices develop large-scale distortions in natural transition. As the wake travels downstream, the energy at the low dislocation frequency decays slowly (in contrast to the rapid decay of other frequencies), leaving the downstream wake dominated by the large dislocation structures. Distinct similarities are found between the periodic forced dislocations and the intermittent dislocations that occur in natural transition. Further similarities of dislocations in different types of flow suggest that vortex or phase dislocations could conceivably be a generic feature of transition in all shear flows.

1. Introduction

A number of investigations have been concerned with the general problem of the development of three-dimensional structure in turbulent shear flows, and with the corresponding implications for mixing in such flows. It is found often that the form and development of such structures can be studied to advantage in the transition region, where some of the smallest scales have not yet developed.

The existence of a transition regime for the wake of a cylinder was first observed by Roshko (1954) in the range of Reynolds numbers of 150–300. In this regime, he found distinct irregularities in the wake velocity fluctuations. It was later suggested by Bloor (1964), on the basis of other work by Sato & Kuriki (1961), that the low-frequency irregularities reflect the presence of three-dimensionalities in the flow that would render the flow turbulent as it travels downstream. Since that time, there has been remarkably little work regarding the transition regime.

In the present investigation, the transition to three-dimensionality in the cylinder wake is studied, but with particular emphasis being placed on the evolution of large-scale structures. It is known that in the three-dimensional transition regime (in the present study this lies roughly between Reynolds numbers from 180 to 260), there are two modes of formation of streamwise vorticity in the near wake, each occurring in a different range of Reynolds number (Williamson 1988*b*; 1991*a*, *b*). Both of these three-dimensional vortex shedding modes involve lengthscales of the streamwise vortex structures which are less than one primary wavelength of the vortex street.

However, it is found in the present paper that the transition to three-dimensionality involves a further phenomenon, and one that is largely responsible for the low-frequency fluctuations observed by Roshko and Bloor, and for the break-up to turbulence in the wake, namely the formation of 'vortex dislocations' in the near wake. Vortex dislocations are generated between spanwise cells of different frequency, when the primary 'Karman' vortices in each cell move out of phase with each other. Across the cell boundaries, a rather contorted web of vortex linking occurs, in what is here termed overall a 'vortex dislocation', in analogy with dislocations that appear in solid mechanics. Dislocations also occur when there is a local phase variation within a larger cell of vortex shedding (in the latter case, a 'two-sided' dislocation is produced, as distinct from a 'one-sided' dislocation which occurs between cells of different frequency). These dislocations grow rapidly in the spanwise direction into large-scale spot-like structures, as they travel downstream. The manner of this spanwise growth seems not unlike the 'transverse contamination' of boundary-layer spots, as described for example by Schubauer & Klebanoff (1956), and Gad-el-Hak, Blackwelder & Riley (1981). Although this paper is concerned with the formation of 'vortex dislocations' which occur naturally during the three-dimensional transition of a bluff-body wake, the primary results to be presented here are obtained from experiments with passively *forced* dislocations, in order that the characteristics of dislocations may be studied in close detail under periodic conditions, without the inherent randomness in space and time associated with natural transition. The principal features of natural three-dimensional transition are presented in a companion paper (Williamson 1992), which includes a more comprehensive study on the natural formation of vortex dislocations.

Although vortex dislocations are found to appear during three-dimensional transition of the wake, they are also a feature of the laminar vortex shedding regime, where they appear in a more ordered fashion than for the transition regime. Dislocations appear between cells of different frequency, and are associated with certain oblique vortex shedding modes (Williamson 1988*a*, 1989*a*; Eisenlohr & Eckelmann 1989; Konig, Eisenlohr & Eckelmann 1990). These laminar oblique-shedding modes, involving cells and dislocations, are influenced by the end boundary conditions. The existence of cells of different frequency appearing near the ends of a cylinder span was shown clearly by Gerich & Eckelmann (1982), and subsequently the phenomenon of 'vortex splitting' between cells of different frequency was demonstrated in a study by Eisenlohr & Eckelmann (1989). In this paper, we define

a 'vortex dislocation' as a vortical region comprising a whole set of 'split' or divided vortices that represent 2π phase variation between neighbouring cells.

The recent surge in experimental studies of vortex shedding patterns, including the existence of cells and dislocations, has prompted studies aimed at modelling the pattern-forming dynamics of wakes. One approach has been to use Guinzburg–Landau equations with diffusive spanwise coupling, and with coefficients evaluated from experiment, as undertaken by Albarede, Provansal & Boyer (1990), Albarede (1991), Albarede & Monkewitz (1992) and Monkewitz, Albarede & Clavin (1990). Their work models remarkably well some of the wake patterns, involving oblique 'phase shocks', chevron patterns, and the effects of the end conditions. Further analysis by Park & Redekopp (1991), using a two-space-dimension Guinzburg–Landau formulation, and by Noack, Ohle & Eckelmann (1991), using a van der Pol oscillator model, have also shown good agreement with wake topologies and dynamics found in experiment. Clearly, there is some effort at present being expended on the modelling of patterns and topologies of vortex formation in wakes.

By way of an introduction to this paper, some typical features of a dislocation will be described from an investigation of a cylinder wake in the laminar regime (referring, in particular, to Williamson 1989*a*). The photographs in figure 23 of this reference show the formation of a (one-sided) vortex dislocation for a vertical cylinder which is moving through water, and which has a higher-shedding-frequency cell in the top part of each photograph relative to the bottom half. Dislocations between two cells were found to involve 'vortex division', whereby a typical vortex of one sign in one cell is divided up and is linked to two vortices of the same sign in the other cell. Such dislocations occur at the beat frequency $(f_1 - f_2)$ between the frequencies of each of the neighbouring cells (f_1 and f_2), and cause modulations in the time traces of velocity fluctuation when a probe is placed between the cells, as was shown in figure 22 of the above reference. At times when the cells were out of phase and the induced velocities almost cancelled, a minimum appeared in the velocity fluctuations. When the probe was placed some spanwise distance either side of the dislocation region, the velocity fluctuations were periodic (and at different frequencies on each side). As one might naturally expect, the corresponding spectra were shown to be periodic well within a frequency cell, but were quasi-periodic close to the cell boundaries. The above typical features for a one-sided dislocation seem to be well-established as general characteristics of one-sided dislocations in several other non-uniform flows.

In the case of the natural three-dimensional transition at higher Reynolds numbers, the appearance of vortex dislocations is not, in general, periodic as in the above example, but seems to be random in time and space. Dislocations also appear as a result of the non-uniform flow close to the ends of bodies in an otherwise uniform flow. However, they are also found in purposefully (or grossly) non-uniform flows past bodies, for example past tapered bodies and cones, or in sheared flows. Phase dislocations in flow patterns are also a feature of other types of flows, for example in free shear flows (both spatially growing and temporally growing cases), in Bénard convection cells, in cloud formation, and in the formation of sand dunes and ripples.

In the case of a free shear layer, Browand and co-workers have for some time been studying the natural and forced development of vortex 'defects' or dislocations in the flow. Browand & Troutt (1980, 1985) demonstrated that dislocations appear naturally in the shear layer between spanwise cells of different frequency, or between cells of similar frequency but which are out of phase with each other. These vortical structures were inferred from velocity measurements using a rake of hot wires along

the span. Browand & Ho (1987) suggested that these defects could be due to very slight non-uniformities in the flow, triggering differences in frequency along the span. Although the defects in the free shear layer observed by Browand *et al.* are found to be produced randomly in space and time, it has proved possible to organize them by acoustic forcing in a wind tunnel (Browand & Ho 1987; Browand & Prost-Domasky 1988, 1990) and so to study their evolution more clearly. A process similar to the vortex splitting (mentioned above) could be inferred from their velocity measurements. The defects cause an increase in the low-frequency velocity fluctuations as the shear layer travels downstream, and it has been found that they are dynamically important in promoting vortex pairing interactions locally in the shear layer (as shown clearly in Dallard & Browand 1991). In fact, the work of Dallard & Browand suggests that the natural density of defects and their tendency to trigger pairing would be sufficient to fill the planform of a shear layer with paired vortices, and thus to be the primary contributor to the growth of the shear-layer thickness. In essence, these defects (or dislocations) seem to be of fundamental importance in the development of such shear layers. Efforts have also been expended to describe such topological effects from theoretical considerations (Yang, Huerre & Coullet 1990; Browand, Legendre & Taniguchi 1989; Yang 1990), and the results are in good qualitative agreement with experimental observations.

Also in a free shear layer, Nygaard & Glezer (1990) have constructed a highly sophisticated heater-strip forcing technique for use in water, with the intention of forcing several different spanwise patterns of vortex formation. By imposing a spanwise phase modulation on the evolving primary vortices, they have induced the primary vortices to split or dislocate at certain spanwise positions in a rather neat manner, and thereby to produce strong streamwise vorticity in the flow. The study has some similarities and is complementary to the flows being studied, using a different technique, by Browand *et al.* Other experiments in a free shear layer by M. Gharib and by K. Williams (at the University of California) have extended the earlier work of Van Atta, Gharib & Hammache (1988), where a vibrating wire created spanwise structures due to interactions of the wire frequency with the natural shedding frequency. They considered the case of a shear layer forced to have different frequencies over each half-span, similar to the experiments described above, further utilizing the control of heater strips. They suggested that vortical structures between cells of different frequency could be part of the fundamental process by which streamwise vorticity is generated in shear flows.

It can be seen from the above that dislocations can readily be generated in free shear flows, but they are also to be expected in another type of flow, namely the non-uniform flow past a body. Gaster (1969, 1971) and recently A. Papangelou & M. Gaster (1991, personal communication), and also Picirillo & Van Atta (1991) have investigated the flows past cones, and it has been found in these studies that cells of different frequency appear, along with the expected dislocation structures between the cells. Agreement between typical experimental results for flow past cones (and cylinders) with computations made on a Connection Machine by Jesperson & Levit (1991) is proving remarkably good for such complex flows. Further work by Lewis & Gharib (1992) has also found interacting cells of different frequency in the wake of a stepped cylinder, which have similarities to the interaction of cells in the wakes of cones. The stepped cylinder is a particularly convenient arrangement for the study of interacting frequencies, because not only are the frequencies reasonably controllable with suitable choice of diameters, but also the interaction will take place in a known region in space (downstream of the step). Finally, different-frequency

cells may be found in the wake of a cylinder placed in a shear flow, and this was shown by Maull & Young (1973) and is also discussed in a review by Griffin (1988). Ongoing work by Rockwell, Nuzzi & Magness (1991) and by Bearman & Szewczyk (1991) seems also to exhibit interacting cells of different frequency in the wakes of bluff bodies with spanwise geometric variations. These studies exhibit phenomena rather similar to those found for the one-sided dislocation in the earlier example (described from figure 23 of Williamson 1989*a*). It seems from all the above that there are a number of detailed investigations presently being conducted on the non-uniform flows past bodies, and primarily in the laminar shedding regime.

The present work has stemmed from studies concerning the three-dimensional aspects of cylinder wakes in principally *uniform* flow conditions. Of particular importance in the present study is the discovery that *vortex dislocations are a fundamental feature of the natural three-dimensional transition* in the cylinder wake, and it is found that very slight phase variations due to the slight near-wake randomness inherent in the three-dimensional modes of shedding can naturally produce dislocations in the wakes of long cylinders. One of the prime characteristics of dislocations is their reasonably fast growth in the spanwise direction, and they seem to trigger a rapid breakdown to turbulence with a broad spectrum within several primary (Kármán) vortex wavelengths downstream of the body. An overview of some aspects of natural three-dimensional transition, as they pertain to the present study of dislocations, is given in §3.

In the present paper, it will be shown that vortex dislocations can be simply triggered artificially, with the intent that the periodic evolution of these structures can more easily be studied as they progress downstream. The dislocations in this case are generated by a small disturbance in the form of a small ring of slightly larger diameter than the cylinder, which is placed at a certain spanwise position on the cylinder, whose wake is otherwise in the laminar regime of shedding. This ring generates a slightly lower frequency of shedding (f_R) than is found over the rest of the cylinder (f), which then results in vortex dislocations appearing at the low beating frequency ($f_D = f - f_R$). The observation that such a ring would generate dislocations originated from a study of possible end conditions for a cylinder (in March 1988), where a large range of endplate diameters was investigated. It was found that even for very small endplates, which were both thin (in the spanwise direction), and had a diameter only slightly larger than the cylinder, the vortices of the main cylinder span did not end smoothly at the endplate, but rather were interacting with the wake of the endplate itself to generate large spot-like structures. Interestingly, as the 'endplate' (or ring) became smaller, so the dislocations became larger, because they scale on the inverse of the dislocation frequency f_D! It was decided at that time to make a preliminary study of these large-scale vortex dislocations for their own sake, with the feeling that whether or not they had a significant connection with natural transition, it was a phenomenon of intrinsic interest. Fortunately, this study has proved most fruitful, as it provides much-needed insight to the naturally occurring dislocations that are a central part of transition. Preliminary examples (shown in colour) of forced dislocations were shown at the November 1988 meeting of the American Physical Society (and subsequently in Williamson 1989*b*, in the *Gallery of Fluid Motion*). Preliminary results linking the forced dislocations with the natural transition have also been presented at the 8th Turbulent Shear Flows Conference (Williamson 1991*c*), and at the 1991 meeting of the American Physical Society, in Scottsdale, Arizona.

General features of the formation of vortex dislocations are given in §4, where

different types of dislocation structures are described. Where a dislocation is formed at the boundary between two cells of different frequency, we call this a 'one-sided' dislocation. Where there is a local phase variation within a larger shedding cell of otherwise constant phase, there will be two boundaries side-by-side where dislocations will form, and we call this a 'two-sided' dislocation. Generally, a one-sided dislocation is an *asymmetric* structure, whereas the stable configuration for a two-sided structure is *symmetric* in plan view.

Wake velocity measurements of forced dislocations are presented in §5, which includes velocity profiles, spectra, and the decay of integrated fluctuation energy downstream. In essence, it is shown that the existence of dislocations drastically alters the distribution of fluctuation energy in the wake. Extensive flow visualization and a discussion of the physical aspects of dislocations is given in §6, followed by phase-locked velocity measurements in §7. In this manner, we are able to deduce instantaneous velocity profiles and to produce contours of velocity in different planes of a typical A-shaped dislocation. From such information, we can discuss features of the overall dislocation velocity field, which are to some extent confirmed by smoke and dye flow visualization. In §8, there follows a discussion on vortex dislocations in non-uniform flows and free shear flows, and also a comparison of some features of vortex dislocations with boundary-layer spots. Finally, and of fundamental significance in this study, a comparison of natural and forced vortex dislocations is made in §9. This is followed by the conclusions in §10.

2. Experimental details

Measurements of velocity fluctuations were made with a miniature hot wire situated in the wake of a cylinder of diameter 0.00104 m, in a 0.152 m (6 in.) diameter circular test section of an open-jet wind tunnel. (Downstream of the 0.61 m long test section, the air is expelled into the atmosphere.) The test cylinder (actually hypodermic tubing) was placed vertically across a diameter at a position about 0.41 m upstream of the end of the test section. The turbulence level was close to 0.1%, with flow uniformity better than 0.3%. A good deal of effort was taken to isolate the cylinder from the tunnel, and to damp out any cylinder vibrations. The cylinder was passed through small holes in the test section, and clamped between felt pads to a tensioning structure outside of, and mechanically separate from, the test section. In addition to this, each cylinder was encased in five-grained polystyrene foam blocks outside the test section (but again not in contact with the test section). Also, the platform, which held the wind tunnel fan, was isolated from any mechanical contact with the settling chamber and test section.

A two-channel hot wire set known as a 'Matilda meter' designed in-house at Caltech (by Dr Brian Cantwell) was used for the velocity measurements. The outputs from one or two hot wires were fed into a HP-3582A two-channel spectrum analyser. Data acquisition was performed using 286- and 386-IBM-compatible computers supported by RC Electronics 'Computerscope' A-D system capable of 1 MHz data capture. Plotting was achieved using 'Betty' (a quality software package) supplied by Dr John M. Cimbala, and colour contour plots were made by taking photographs of the screen of an IRIS computer in the laboratory of Dr Dean Taylor (at Cornell). Software comprised a finite-element package, normally used in structural analysis, called PATRAN.

Flow visualization was conducted in an X–Y Towing Tank (at Caltech), and in a wind tunnel with a 0.305 m (1 ft) square test section (at Cornell). The towing tank

operates much like a giant computer X–Y plotter, and can impart arbitrary unsteady trajectories to bodies which are towed within the fluid in the glass tank (of length 5 m and cross-section 1×1 m). Cylinders of diameter 0.00328 and 0.00657 m were towed along the length of the tank, and the shed vorticity was visualized using laser light which excited fluorescein dye washed off the surface of the cylinders. Where two-colour visualization is needed, Rhodamine dye is also used. In the case of stereoscopic flow visualization, two synchronised Nikon F3HP motordrive cameras were used. They were linked to a function generator which output TTL pulses at a prescribed low frequency of typically around 0.3 Hz.

In most of this work, forced dislocations are created in a wake which is in the laminar vortex shedding regime at a Reynolds number of 120, unless otherwise stated. The origin of the coordinate system is fixed on the axis of the cylinder. The x-axis is downstream, the y-axis is perpendicular (defined as transverse) to the flow direction and to the cylinder axis, and the z-axis lies along the axis of the cylinder (defined as spanwise). Unless otherwise stated, the data for the transverse profiles are measured for positive y, and its mirror image used for negative y, under the assumption of symmetry.

3. Overview of some aspects of natural three-dimensional transition

The appearance of large-scale dislocations is found to be a fundamental aspect of the three-dimensional transition in the wake. These dislocations are directly related to certain characteristics of the transition wake, of which an overview will be given briefly here.

In the transition regime, it has been found that there are differences in the development of streamwise vorticity in the wake of bluff bodies as compared with the 'unseparated' wake from a splitter plate. These differences arise from the presence of the bluff body in the former case, which causes the main part of the streamwise vorticity to originate primarily from a spanwise instability of the primary vortices or '2-D rollers' (Williamson 1988*b*, 1991*a*, *b*). Over a range of Reynolds numbers (Re), two modes of three-dimensionality are found, and the appearance of each mode, as we increase Reynolds number, corresponds with a discontinuity in the Strouhal–Reynolds number relationship, as can be seen in figure 1. Above $Re = 180$, there is a discontinuous change in the wake formation, as the primary wake vortices become unstable and generate large-scale vortex loops, as shown typically in figure 2(*a*). (These loops correspond with what Gerrard 1978 described as 'fingers'.) This 'mode A' three-dimensional shedding corresponds with Strouhal curve A in figure 1. Between $Re = 230$ and 260 there is a transition to a mode B three-dimensional shedding involving the inception of finer-scale streamwise vortex structure (shown in figure 2*b* to the same scale as *a*), with a shedding frequency corresponding to curve B in figure 1. At this discontinuity there is no hysteresis (as occurs at the first discontinuity), and it is found that two modes of vortex shedding (modes A and B) alternate in time. There are thus two stages in the transition to three-dimensionality in the wake of a bluff body, each of which is associated with a different scale of streamwise vortex structure, and with a different vortex shedding frequency. These 'small-scale' streamwise structures in the transition of a separated wake have some similarity with such structures found previously in a mixing layer (Bernal & Roshko 1986), and in the unseparated wake downstream of a splitter plate (Meiburg & Lasheras 1988).

Striking differences in the character of the wake between the laminar and the

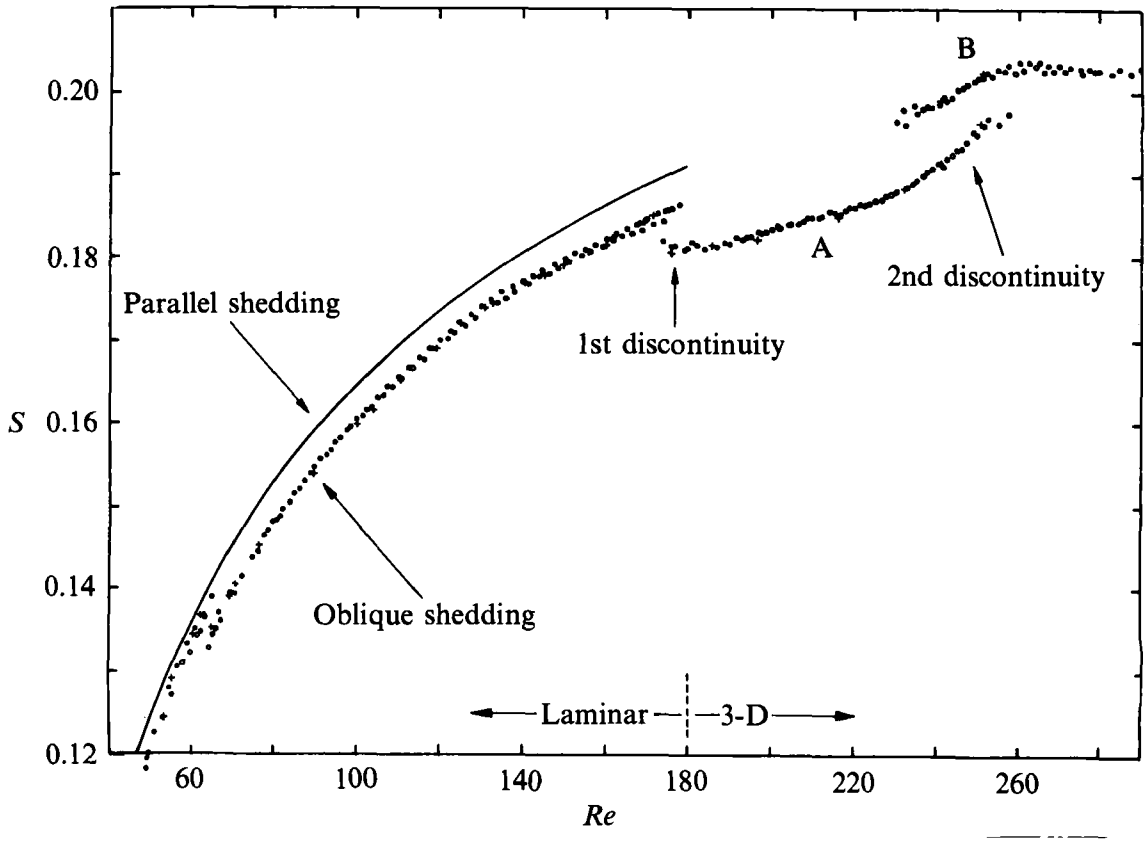

FIGURE 1. Strouhal number versus Reynolds number over the laminar and transition regimes. The two discontinuities indicate the existence of two stages in the development of natural transition, and are associated with the inception of different modes of three-dimensional shedding (modes A and B). ○, $D = 0.104$ cm ($L/D = 140$); ●, $D = 0.061$ cm ($L/D = 200$); +, $D = 0.051$ cm ($L/D = 240$).

transition regimes can be seen in figures 3 and 4. The transverse profile of $u'_{\rm rms}$ fluctuations for $x/D = 30$ in figure 3(*a*), when there is laminar shedding ($Re = 152$), shows two peaks (on either side of the wake centreline) corresponding to the two organized rows of laminar vortices travelling downstream past the probe. The 'three-dimensional turbulent' case of $Re = 183$, on the other hand, shows much larger overall fluctuation energy, with a maximum in the wake centre. The central maximum in the $u'_{\rm rms}$ profile is due to large-scale structures, which principally contribute to the fluctuations downstream. These structures extend over large numbers of primary vortices, and have a structure that is approximately similar on both sides of the centreplane (x–z plane). This 'transverse symmetry' is further confirmed from twin-hot-wire measurements in Williamson (1992). A maximum fluctuation velocity is induced in the centreplane, directly between the two halves of the large structure. Figure 3(*b*) shows that the level of the $u'_{\rm rms}$ fluctuations (measured at $y/D = 1.0$) decays downstream much slower for the three-dimensional (turbulent) shedding case than for the laminar case (which decays exponentially beyond about $x/D = 10$). The distribution and magnitude of turbulent wake fluctuations are clearly very different from the laminar case.

The differences in the levels of $u'_{\rm rms}$ fluctuations for transition and laminar flow

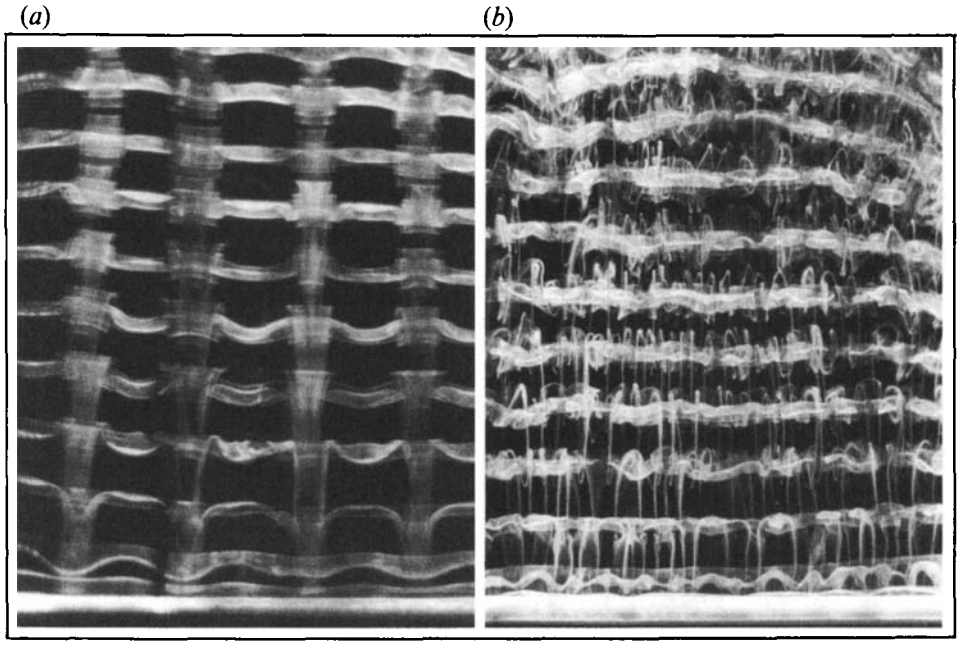

FIGURE 2. Modes A and B three-dimensional vortex shedding. (*a*) Mode A represents the inception of streamwise vortex loops, for $Re = 180$ and above. These loops are caused by the deformation, during the process of shedding, of the primary 'Kármán' vortices. Spanwise lengthscale is around 3 diameters, or $\frac{3}{5}$ primary wavelengths. (*b*) Mode B represents the formation of finer-scale streamwise vortex pairs, for $Re = 230$ and above. These are due to the rather more-uniform vortex deformation. Spanwise lengthscale is around 1 diameter, or $\frac{1}{5}$ primary wavelengths. Note that both of these photographs are to the same scale.

correspond in figure 4 with the much larger velocity fluctuations downstream for the transition Reynolds number ($Re = 183$) than for the laminar case. These low-frequency irregularities are basically the same phenomenon that was originally observed by Roshko (1954). Subsequently Bloor (1964) suggested that they were probably due to three-dimensionalities in the flow. In figure 4, one can see that the large fluctuations are of much lower frequency than the upstream vortex shedding frequency, and are related to the occurrence of the intermittent 'glitches' appearing in the time traces further upstream at $x/D = 10$. These intermittent glitches are caused by the formation of vortex dislocations (as shown later in figure 38). In summary, it is the growth of these dislocations into massive structures downstream that causes the large velocity fluctuations at low frequency, and the relatively slow decay of fluctuation kinetic energy as compared with the laminar wake.

It should be mentioned that there are similarities in some of the above with experiments on the transition of a wake from a symmetric airfoil at zero incidence. Sato (1970) also found low-frequency irregular fluctuations in natural transition, which were a maximum on the wake centreline. From his measurements of orthogonal velocity components, he deduced that these large irregular fluctuations were due to large-scale three-dimensionalities, which corresponds directly with the case here. Also, of significance to the present work, is an investigation by Williams-Stuber & Gharib (1990), who conducted experiments on the wake of a symmetric airfoil in water, with a means to introduce more than one frequency into the wake using heater strips. The fluctuation profile for their chaotic case (involving three

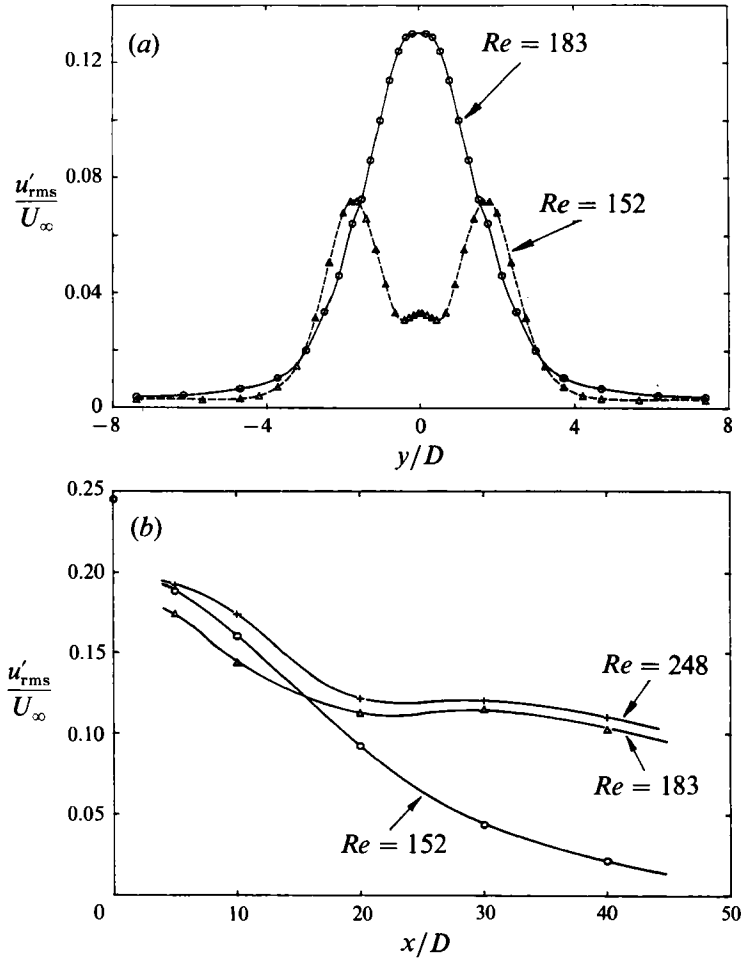

FIGURE 3. Velocity fluctuations for the natural three-dimensional transition wake versus the laminar wake. (*a*) Transverse profiles of (u'_{rms}/U_∞) velocity fluctuations, showing the marked contrast between the laminar wake ($Re = 152$) and three-dimensional transition wake ($Re = 183$). $x/D = 30$. (*b*) Downstream decay of (u'_{rms}/U_∞), showing the much slower decay for the three-dimensional transition wake ($Re = 183$), as compared with the laminar wake ($Re = 152$). (Measurements are made at $y/D = 1.0$).

different frequencies) is similar to figure 3(*a*), and they found that the central peak is associated with the low interaction (or beat) frequencies. This is consistent with the conclusions of Sato, when he used two-frequency forcing.

Visualization of naturally occurring vortex dislocations in the three-dimensional wake transition are shown in figure 5, where we can see a two-sided dislocation travelling downstream on the left, and a further dislocation gradually forming in the near wake on the right of the photograph. Both of these are due to a local phase dislocation within a cell which is otherwise shedding at a reasonably constant phase along its length. Much of the present paper is given over to a study of such two-sided dislocations, primarily those that are forced. At the end of the paper in §9, having discussed forced dislocations in detail, we shall return to the natural transition case and make a direct comparison between natural and forced dislocations.

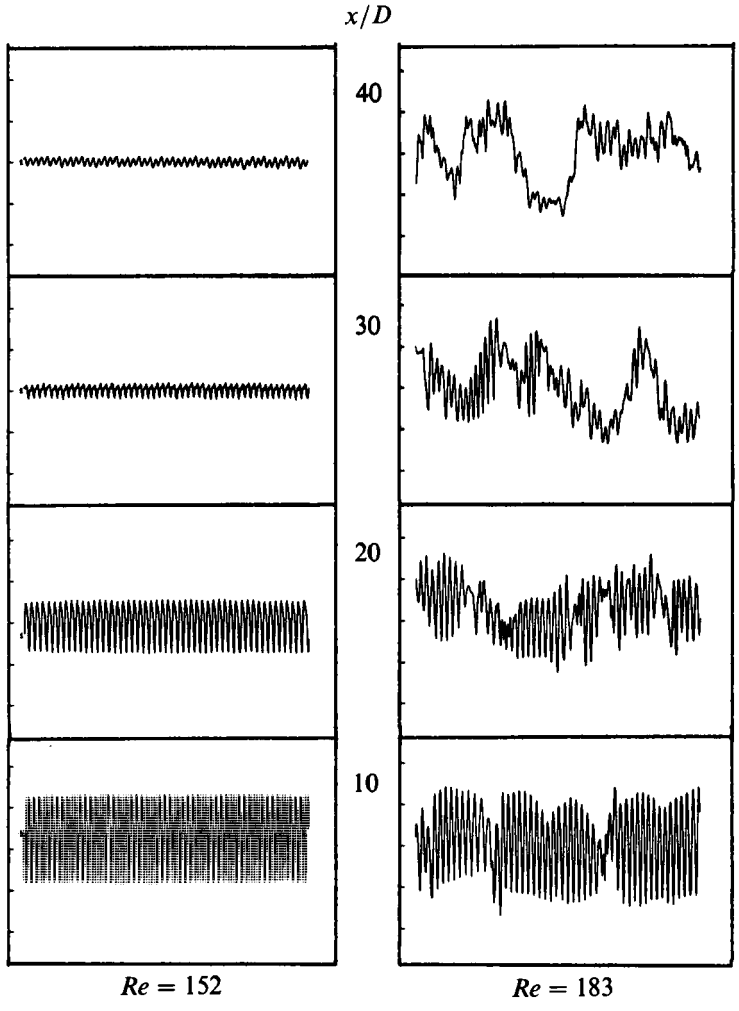

FIGURE 4. Downstream decay of u' fluctuations for the three-dimensional transition and laminar wakes. The time traces of velocity fluctuations on the left for the laminar wake ($Re = 152$) show a rapid decay of energy, in contrast with the three-dimensional turbulent wake on the right ($Re = 183$), for which the energy at the shedding frequency rapidly gives way to large low-frequency oscillations. The origin of these large oscillations downstream ($x/D = 40$) comes from the 'glitches' in the time traces found upstream ($x/D = 10$), and are due to the formation of natural vortex dislocations. (Time traces are scaled correctly relative to each other, although the scale is arbitrary.)

4. General features of the formation of vortex dislocations

It is often found that vortical structures which occur in shear flows can conveniently be investigated by forcing them to appear in a controlled manner. An example of this is the generation of turbulent spots in a boundary layer either singly or periodically by using roughness elements on the boundary surface, by initiating an electric spark on the surface, and also by fluid injection (Schubauer & Klebanoff 1956; Gad-el-Hak *et al.* 1981; Wygnanski, Sokolov & Friedman 1976; Cantwell, Coles & Dimotakis 1978). A further example of this approach is the forced generation of 'defects' by Browand and co-workers for the free shear layer.

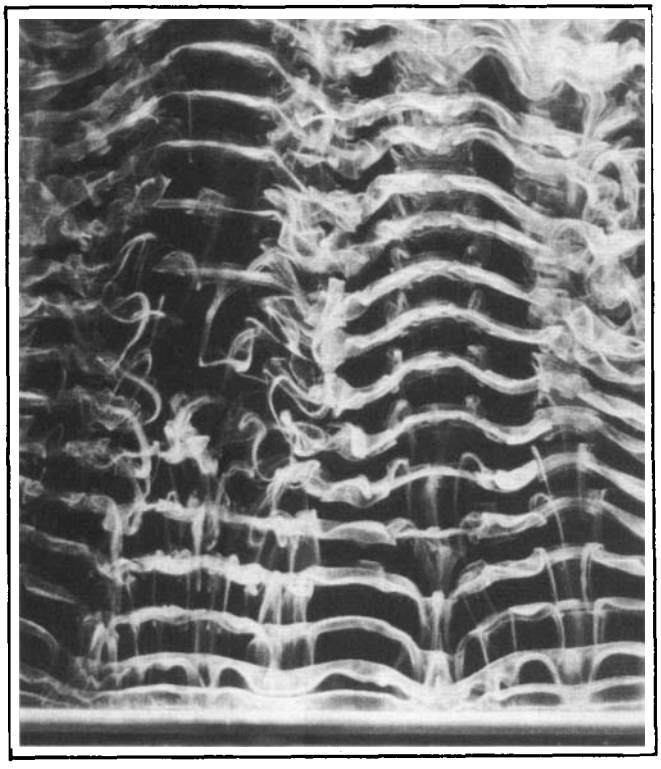

FIGURE 5. Natural formation of 'vortex dislocations' as part of the transition process. Symmetric two-sided dislocations appear when there is a local phase variation of the shedding, causing out-of-phase vortex formation to each side. The photograph shows a vortex dislocation travelling downstream on the left and a further dislocation forming on the right. Flow is upwards, and the horizontal cylinder is shown as the thick white line at the bottom. $Re = 210$.

In the present case, vortex dislocations are produced artificially in an otherwise laminar wake ($Re = 120$) by using a small disturbance at a local spanwise position, in the form of a ring of slightly larger diameter than the cylinder diameter. The ring that is used principally in this study is half a cylinder diameter (D) in spanlength, with a ring diameter of $1.5D$. As described earlier, this causes locally a vortex frequency of slightly lower frequency (f_R) than over the rest of the span (f), and induces two-sided dislocations to appear. It is not clear ahead of time whether these pairs of dislocations on either side of the ring will be in phase or out of phase. This question is considered below.

Preliminary investigations of forced two-sided dislocations showed that it is rather important to match the shedding frequency of the cylinder span on either side of the ring. This requires matching the conditions at the ends of the complete cylinder span, because these effects can influence the angle of oblique vortex shedding and thereby the shedding frequency (the connection between angle and frequency are discussed in Williamson 1989*a*). Observing patterns of two-sided dislocations in figure 6, we can see that by deliberately organizing the oblique angles and frequencies to be different (f_1 and f_2) on each side of the ring disturbance in figure 6(*a*), we can generate dislocations on the right (of the ring) at a beat frequency ($f_{D1} = f_1 - f_R$) which is different to the other side ($f_{D2} = f_2 - f_R$). (A schematic of this situation is shown in

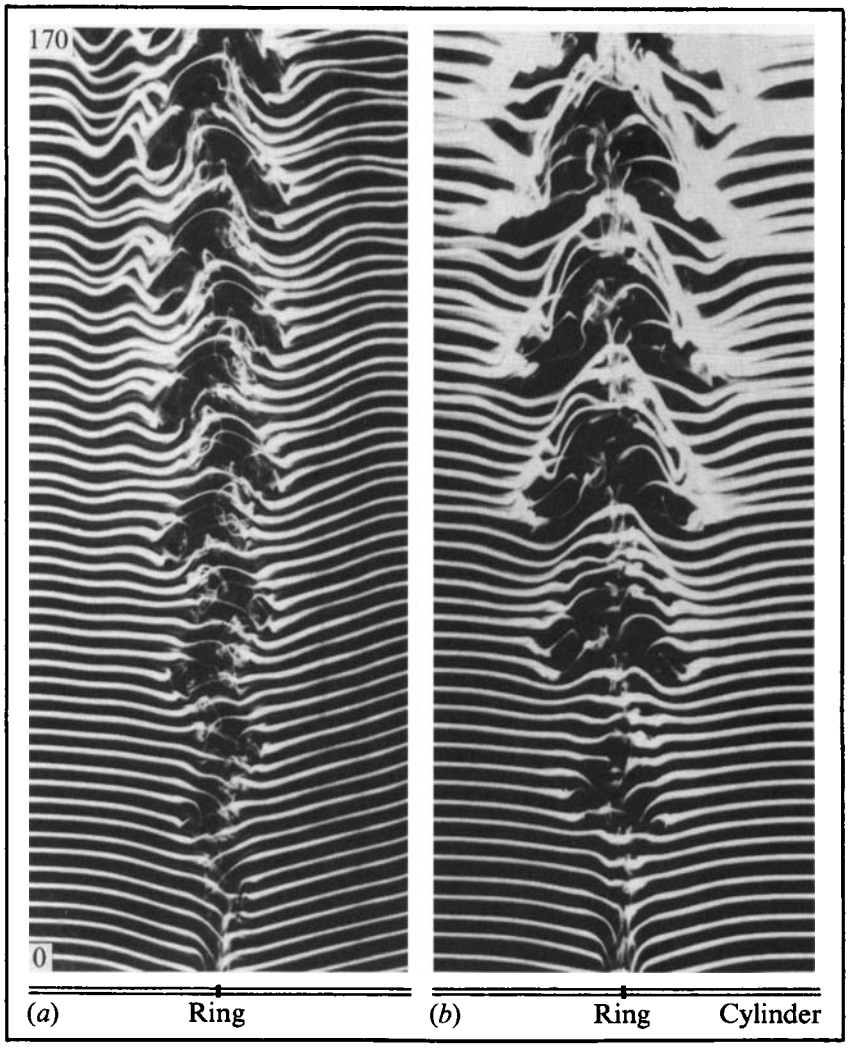

FIGURE 6. Two-sided dislocations: stable versus transient configurations. (*a*) Transient (out-of-phase) two-sided dislocation. This is a snapshot that captures a moment when the dislocations on each side are out of phase. It is the result of a transient phase relation between the two dislocations, because the dislocation frequency on each side is different. (*b*) Stable (in-phase) symmetric two-sided dislocation. This appears indefinitely when the dislocation frequency on each side of the ring is the same, and is the preferred stable configuration. The numbers on the left show values of x/D.

figure 9*b*.) Thus the dislocations on each side of the ring will move in and out of phase with each other at the very low beat frequency of $(f_{D1}-f_{D2})$ which is the same as (f_1-f_2). Although from one photograph as in figure 6(*a*), it would be tempting to suggest that this particular antisymmetric arrangement of dislocations is an equilibrium pattern, it is in fact a transient pattern, and the photograph happens to catch the two rows of dislocations when they are out of phase with each other. In the wind tunnel, with actual shedding frequencies (f_1 or f_2) of around 300 Hz, one could arrange for the transient pattern to move in and out of phase at a frequency of around 1 Hz, and this oscillation was readily observable on some of the instrumentation used during the experiment (RMS meter, spectrum analyser and

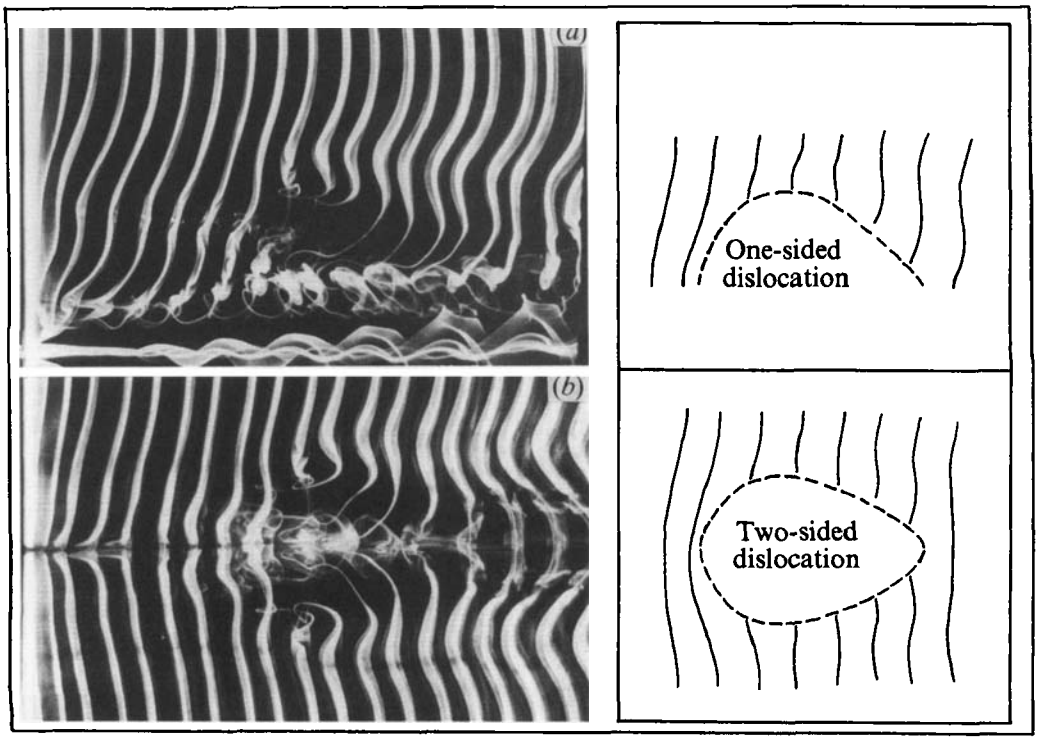

FIGURE 7. Similarities of one-sided and two-sided dislocations. A one-sided vortex dislocation formed near the end of a cylinder span (bottom) is shown in (*a*), and is due to a lower frequency cell near the end (from Williamson 1989*a*). A two-sided dislocation with a lower frequency in the centre (horizontally) is shown in (*b*). In both cases the flow is to the right. The two cases are remarkably similar in their structure and evolution.

oscilloscope). By careful manipulation of the conditions, it was possible to induce the symmetric pattern of the two dislocations in phase with each other, as in figure 6(*b*). This configuration is found to be 'stable', in the sense that it can continue indefinitely.

It should be noted from the dye visualization in figure 6 that the symmetric structures seem still to be forming far downstream at $x/D = 170$, although the energy in the fluctuations is only small at this point. The studies by Cimbala, Nagib & Roshko (1986) demonstrated clearly the fact that smoke visualization carried downstream may exhibit only the 'skeleton' of what evolved further upstream. However, the visualization later in figure 30, introducing smoke at $x/D = 75$, suggests that the structures still retain some energy, at least to $x/D = 140$.

One might question whether the symmetric two-sided dislocation should indeed occur, or whether even the slightest fraction of a frequency difference on either side of the ring will cause the two rows of dislocations to fall out of phase. In fact, it proved relatively simple to have the stable configuration continue indefinitely, a situation which is shown clearly in §7 where the phase-locked measurements naturally required solidly steady conditions. It is believed that the reason for this is that the shedding on one side of the ring exerts a (Biot–Savart) induced-velocity 'forcing' on the shedding of the other side, such that the flow on each side becomes synchronized in-phase. The symmetric two-sided dislocation is thus stable.

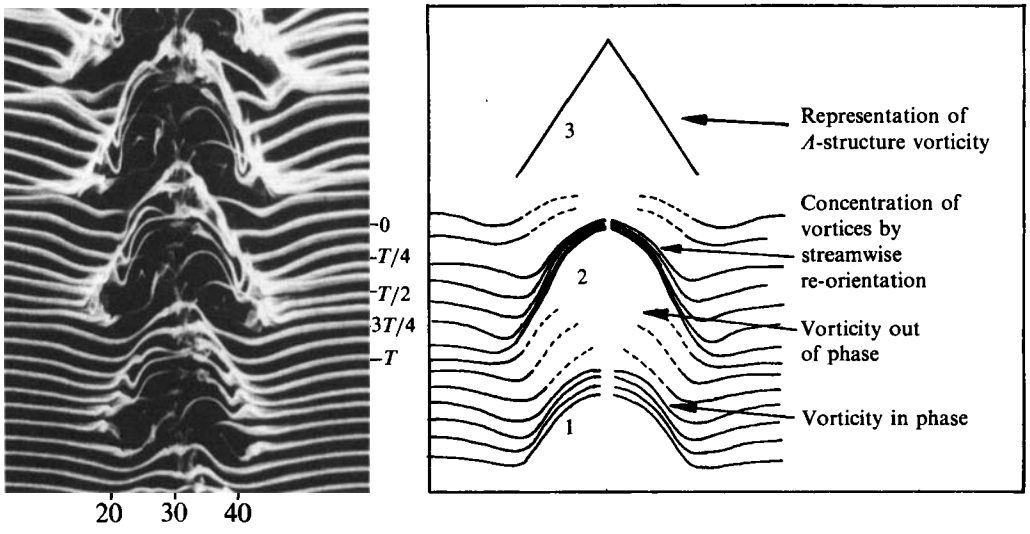

FIGURE 8. Schematic of the evolution of dislocations, and their simplified representation. The diagram on the right is drawn to correspond with the evolving symmetric dislocations on the left (flow upwards in the figure). The downstream structure is represented, for the purpose of the next figure, by a single A-structure of concentrated vortices. (The numbers and letters around the photograph are for use in figure 26.)

The symmetric two-sided type of dislocation is the one that seems to be observed most frequently in the natural three-dimensional transition, although its occurrence in this case is not periodic as for the forced situation. Another type of dislocation that appears in the natural transition is the one-sided dislocation, which is observed between spanwise cells that become out of phase with each other. In natural transition, such a scenario is possible because of the competition between modes A and B three-dimensional shedding, which both have different frequencies. In the laminar regime too, such one-sided dislocations are observed primarily near the end boundaries, where there exists an end cell of lower frequency than occurs over the rest of the span. Observation of a one-sided dislocation, shown in figure 7(*a*) and taken from Williamson (1989*a*), may be compared with a two-sided dislocation shown in figure 2(*b*). (Such a one-sided dislocation may similarly be seen in what was described as a 'knot' of turbulence by Slaouti & Gerrard 1981.) The vortex linking, spanwise growth and general evolution of the one- and two-sided dislocations are remarkably similar, a fact which is perhaps not unexpected.

A brief schematic summary of the evolution of a large-scale A-structure is shown in figure 8. In each overall dislocation there are vortices on each side of a cell boundary which meet up primarily in phase, while others will divide themselves and be distinctly out of phase with those on the other side of a cell boundary. The vortices in a dislocation convect rapidly downstream relative to the vortices in the street to either side. This is because the vortex elements in a dislocation are highly distorted in three dimensions, and result in less upstream induced velocity than is present in the more-organized vortex street. This aspect is shown in the photograph, where the relative upstream motion of the street vortices causes the formation of a A-structure, and is represented schematically by the lines in figure 8. We should note that the vorticity in the Kármán vortices has diffused more rapidly than the dye in the photograph, and at these downstream locations (in the vicinity of $x/D = 70$) there is

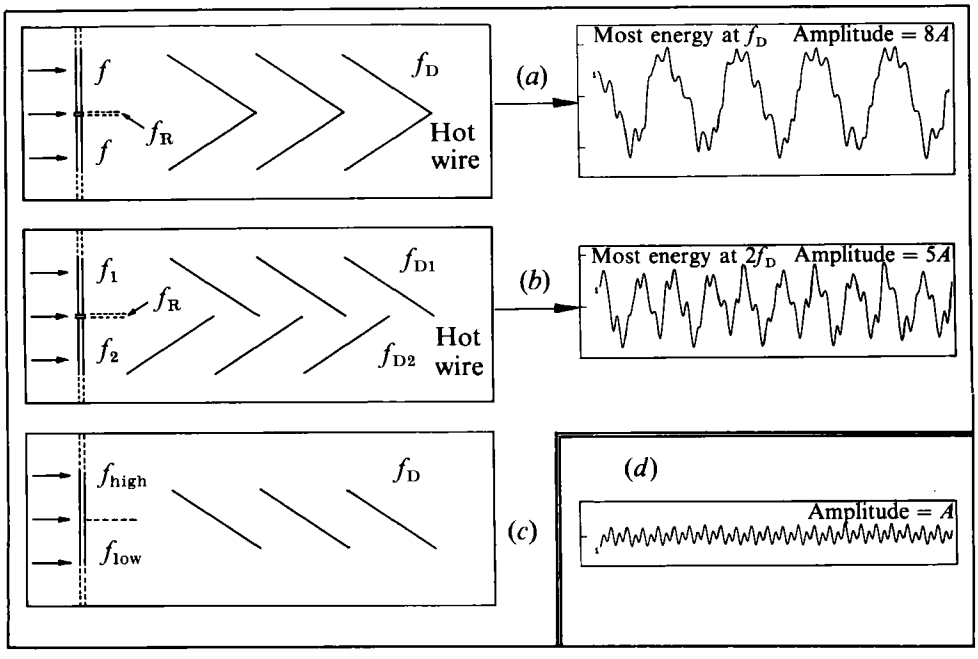

FIGURE 9. Classification of three different types of dislocations, and their velocity fluctuations. On the left are shown representations of certain types of dislocation, drawn such that each line represents a region of concentrated vortices, in the manner of the previous figure. (*a*) Symmetric (in-phase) two-sided dislocation (stable configuration). It gives a large velocity fluctuation (at $x/D = 40$, $y/D = 0$, $z/D = 0$) of around 8 times that found in a normal laminar street without dislocations at a similar location, shown in (*d*). (*b*) Antisymmetric (out-of-phase) two-sided dislocation (transient configuration). (*c*) One-sided dislocation.

very little fluctuation energy left in the vortex street (as shown by Cimbala *et al.* 1988), although the energy in the large structures (shown in §5) can be an order of magnitude larger than in the street.

Different configurations of dislocations are shown in figure 9, where the large-scale structures are represented by lines, in the manner of figure 8. To summarize, if the frequencies are the same on both sides of the ring, as in figure 9(*a*), then symmetric (two-sided) A-structures will evolve downstream at a frequency $f_D = f - f_R$. If, however, the frequencies to each side are different (f_1 and f_2) then the two resulting rows of dislocations will have different frequencies, $f_{D1} = f_1 - f_R$ and $f_{D2} = f_2 - f_R$, and the antisymmetric configuration shown in figure 9(*b*) is then a transient state. A third possibility is simply the one-sided dislocation structures that form at an angle to the flow in figure 9(*c*) due to the interaction between two cells of different frequency (in this case $f_D = f_{high} - f_{low}$). It should be noted that these one-sided dislocations are angled with the orientation as shown, when the high and low frequencies are as indicated.

In figure 9, we can also qualitatively compare the velocity fluctuations at the centreline of the patterns for each of the two-sided configurations. At $x/D = 40$, the symmetric dislocation yields large fluctuations, at a frequency of f_D, with an amplitude of the order of 8 times that for a normal wake. What is rather interesting is that the two-sided antisymmetric dislocation yields fluctuations at a frequency of $2f_D$ rather than f_D, and at a smaller amplitude of around 5 times the normal wake fluctuations. The reason for these differences is that in the symmetric case the large-

scale structures are acting in phase with each other as they pass the probe in the centre of the pattern, whereas for the antisymmetric configuration, the two rows of dislocations are not inducing velocity fluctuations at the probe in unison, so the amplitude is diminished. For the latter case, it can be simply seen from the symmetry of the pattern that the large fluctuations will occur at (closely) twice the frequency f_D.

In the next Section, we shall look at wake velocity measurements for the two-sided symmetric dislocations, and it will be shown that, although the dislocation upstream is initiated as a small effect, its rapid spanwise growth further downstream causes surprisingly large effects on the wake measurements, in a manner similar to that for natural transition.

5. Effect of vortex dislocations on wake velocity measurements

5.1. *Mean and fluctuating velocities*

Both the mean and fluctuating velocities are significantly influenced by the presence of two-sided vortex dislocations, as can be seen from figure 10. The mean spanwise profiles on the left show that there is an increase in the wake velocity defect in the neighbourhood of the disturbance at $x/D = 5$, although this trend is dramatically reversed further downstream, which seems at first rather surprising. The almost jet-like effect in the dislocation region is due to the relatively fast upstream velocities that remain in the more-organized street wake to each side of the profile. Another aspect to observe in this figure is the rapid spanwise growth of the dislocation region. At $x/D = 40$, this region becomes about 30 diameters wide, which is around 6 primary wavelengths, and is far larger than the width of the ring disturbance (also marked in the figures). It can also be seen on the right of the figure that the maximum $u'_{\rm rms}$ fluctuations in the centre of the profile at $x/D = 40$ are an order of magnitude larger than the fluctuations outside the dislocation region, in an otherwise normal wake. Lastly, there are noticeable 'substructures' indicated by the waviness of the $u'_{\rm rms}$ profiles, which will be discussed later.

Consistent with the above, the transverse velocity profiles in figure 11 also exhibit large effects due to the presence of the dislocations. Upstream, the mean wake profile behind the ring (on the left for $x/D = 5$) is similar to that for a normal wake, although the momentum defect is in fact larger, whereas further downstream (at $x/D = 40$ and 80) the opposite effect occurs, with the dislocation wake also becoming wider. The fluctuations due to the dislocations (on the right of the figure) also grow much larger than those from a normal vortex street and, in a manner similar to that for the natural three-dimensional transition, there is a central maximum in the profile, because of the transverse symmetry of large-scale structures, mentioned earlier.

The velocity–times traces in figure 12 show that the peak in the fluctuation profile is associated with the rapid growth of oscillations at the low dislocation frequency ($f_D = f - f_R$), which swamp any remaining oscillations at the original shedding frequency. These large oscillations contrast sharply with the small fluctuations found in a normal wake at similar downstream locations. The growth of energy at the dislocation frequencies can also be shown clearly from spectral measurements of the velocity.

5.2. *Spectral measurements and fluctuation energy*

A marked change in the type of spectra as we traverse the probe spanwise (at fixed $x/D = 40$ and in the wake centreplane) can be seen in figure 13. Outside the influence

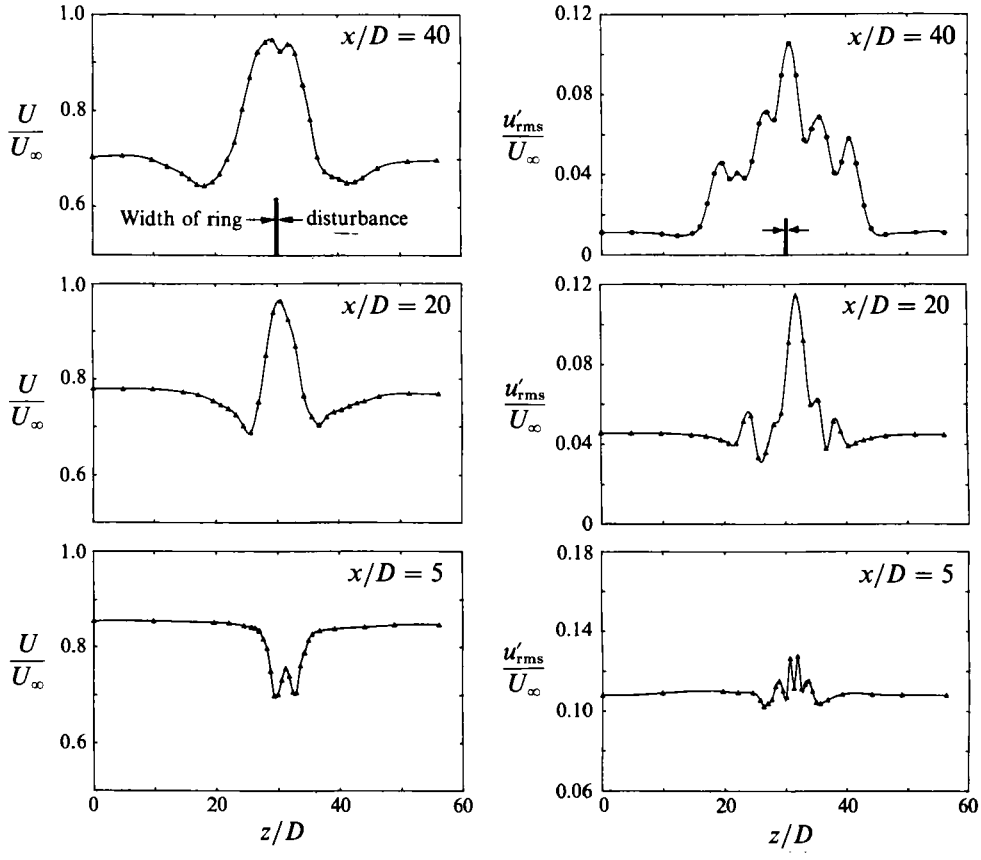

FIGURE 10. Mean and fluctuating velocity profiles (spanwise). On the left are shown mean velocity (U/U_∞) profiles taken in the centreplane of the wake ($y/D = 0$) at certain downstream locations (different x/D). Downstream, it is clear that the effect of the ring disturbance extends far wider than the width of the ring itself. On the right are shown fluctuation (u'_{rms}/U_∞) profiles, which demonstrate the rather large fluctuations associated with the presence of the dislocations.

of the dislocations, the energy lies primarily at the normal vortex shedding frequency and its first harmonic, f and $2f$. (It should be noted that the maximum is found at $2f$ because the probe lies midway between the two rows of vortices in the street, and will get the same-sign contribution to the fluctuations from vortices in either row.) As the probe is moved into the influence of the dislocations (the centreline of the dislocations is defined here as $z^*/D = 0$), there is an increase in energy at the ring shedding frequency and its first harmonic, f_R and $2f_R$ and at the large-scale dislocation frequency $f_D = f - f_R$. When the probe is located centrally in the path of the dislocations ($z^*/D = 0$) then the principal energy lies clearly at frequency f_D, with other peaks at combination frequencies comprising f_D and f_R.

If we fix the spanwise position of the probe near the centreline of the dislocations ($z^*/D = 1$) and traverse it downstream, then again the dislocation frequency f_D rapidly takes over, as shown in figure 14. In the path of the dislocations, it can be seen that the energy at f_D exceeds that at the ring frequency $2f_R$ just beyond $x/D = 10$, and further downstream it becomes far larger than the peak energies found in the normal wake.

Finally, we can interpret the spectral peaks in a typical spectrum (for example

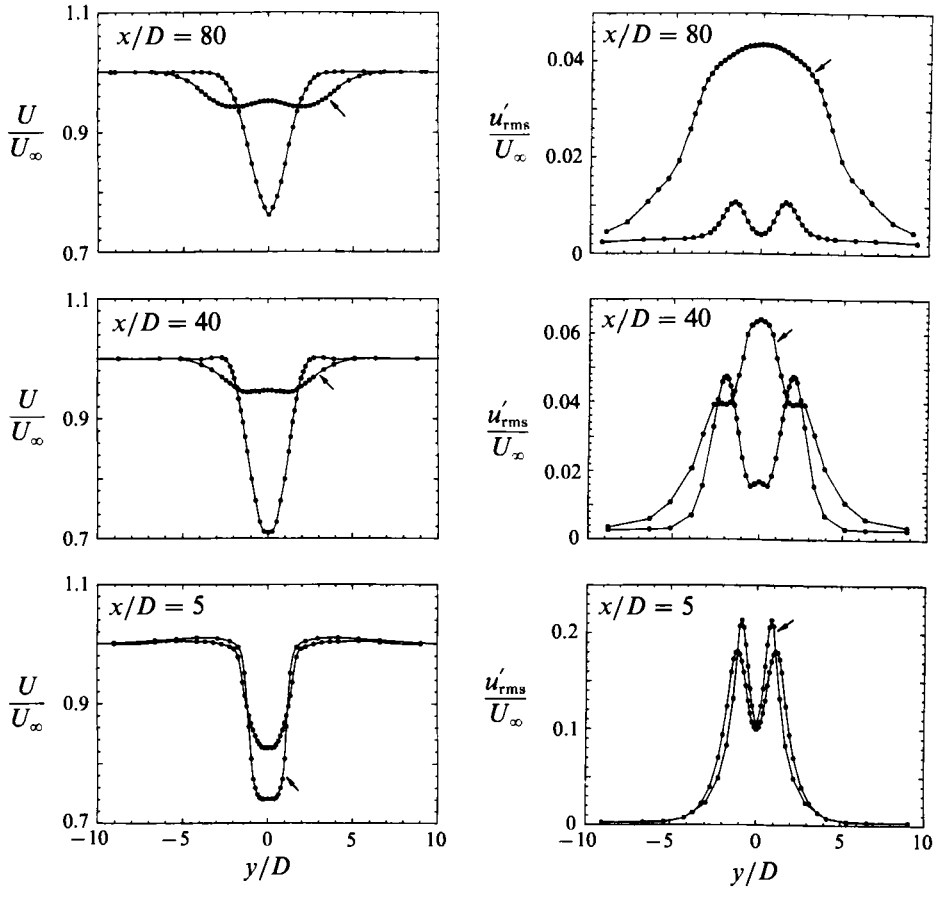

FIGURE 11. Mean and fluctuating velocity profiles (transverse), with and without dislocations. On the left are shown mean velocity (U/U_∞) profiles, where the probe is traversed in the transverse direction (y/D). Downstream, the wake with dislocations (open symbols, marked with an arrow) is wider, with markedly less momentum defect, than the normal laminar wake (solid symbols). On the right are shown velocity fluctuation ($u'_{\rm rms}/U_\infty$) profiles, which demonstrate the much larger fluctuation level of a wake with dislocations, and the characteristic central peak in the profiles downstream. We can note the similarity with profiles for natural three-dimensional transition from the laminar state (see figure 3).

figure 14, at $x/D = 40$ for the wake with dislocations) as all being due to combinations of $f_{\rm D}$ and $f_{\rm R}$, which is perhaps the logical choice of frequencies in the path of the dislocations. All of the principal peak frequencies in this figure can be simply demonstrated to be combinations of the harmonics of $f_{\rm R}$ with the harmonics of $f_{\rm D}$, and can be written in this case as

$$nf_{\rm R} + (m-3n)f_{\rm D} \quad \text{where} \quad n = 0, 1, 2, \ldots, m = 1, 2, 3, \ldots$$

with almost no energy observed at other frequencies. (As expected, all of these peaks can alternatively be written solely in terms of frequencies f and $f_{\rm R}$, since these can be considered the basic frequencies in the problem.) Essentially, all that the above shows is that in the path of the dislocations, the principal interactions are between a waveform at the low frequency of $f_{\rm D}$ with another higher-frequency waveform at the ring frequency $f_{\rm R}$, and we can interpret such a quasi-periodic spectrum in this manner.

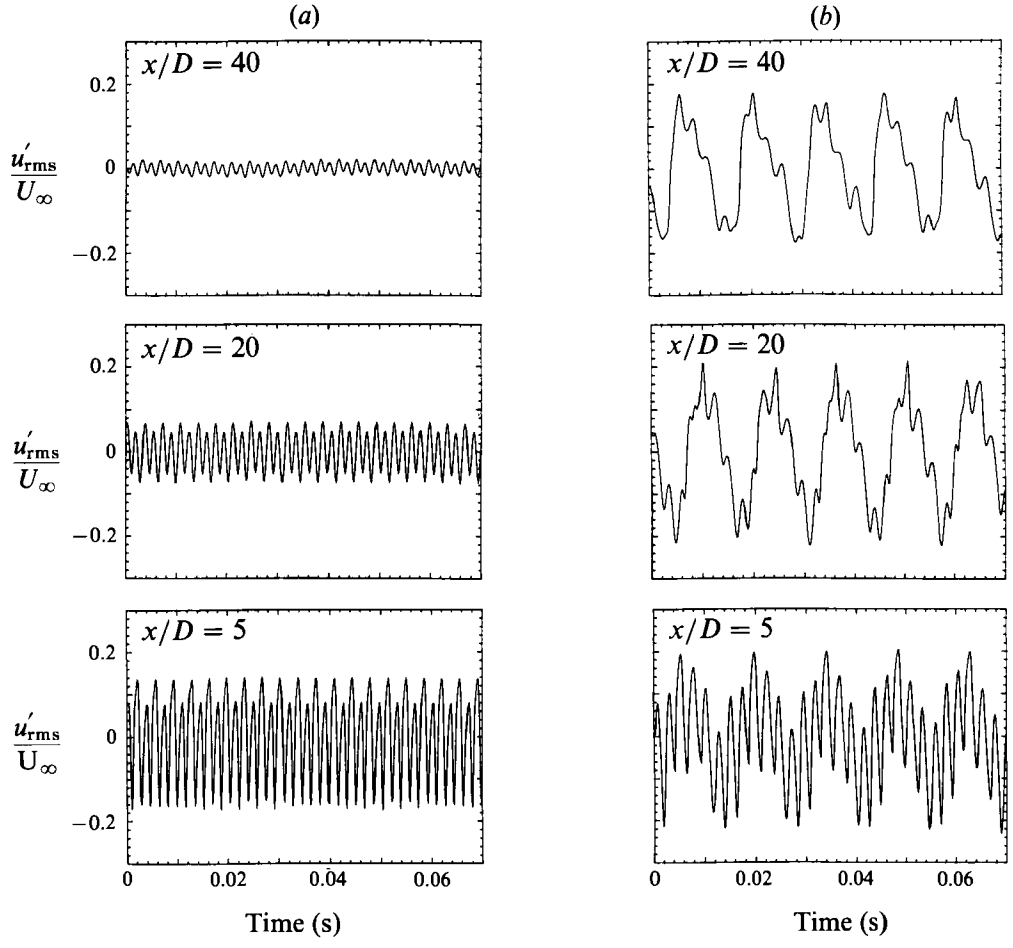

FIGURE 12. Velocity signals, with and without dislocations. The large low-frequency fluctuations in a wake with dislocations (*b*) may be contrasted with the rapid exponential decay of high-frequency fluctuations for the normal street wake (*a*). (y/D close to 0).

It is of interest to use spectral measurements to form fluctuation profiles for specific frequencies, as shown in the spanwise and transverse energy profiles of figures 15 and 16. In this case we plot the total energy $(u'_{\rm rms}/U_\infty)^2$ versus the energies deduced from the peak values in the spectrum at the shedding frequencies of the normal wake (f), at the ring shedding frequency ($f_{\rm R}$), and at the large-scale dislocation frequency ($f_{\rm D}$). In each case we take into account the fundamental frequency and its first harmonic only (e.g. f and $2f$ only). The spanwise fluctuation energy profiles show distinct changes as the flow progresses downstream. At $x/D = 20$, in the path of the dislocations (near to $z/D = 31$), the principal component of energy is at the dislocation frequency $f_{\rm D}$, with some energy at $f_{\rm R}$. Obviously as we move out to the sides into the normal wake, we expect the energy at $f_{\rm D}$ to diminish along with $f_{\rm R}$, and the energy at the normal shedding frequency f to take over. At $x/D = 40$, shown in figure 15, practically all of the energy of fluctuation is at the dislocation frequency $f_{\rm D}$. An interesting point to mention is that the waviness in the profile, suggesting substructures in the flow, is again noticeable. It can be seen that this waviness is related to the overall dislocation energy at $f_{\rm D}$ rather than connected with frequencies f or $f_{\rm R}$.

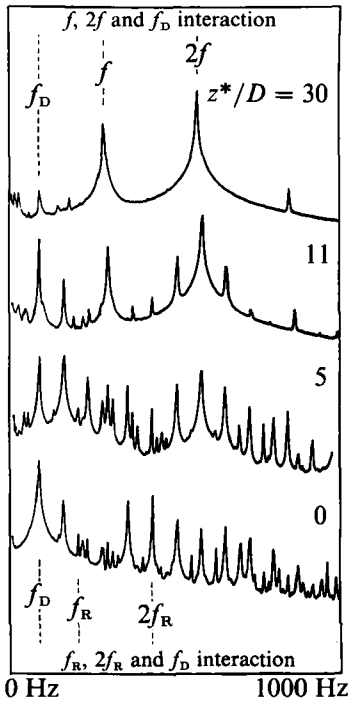

FIGURE 13. Spectra at different spanwise locations. These spectra demonstrate how the fluctuation energy at the dislocation frequency (f_D) takes over from the energy at the vortex street frequency (f, $2f$) as the probe is traversed into the dislocation region. The interaction between f, $2f$ and f_D gives way to interaction between f_R, $2f_R$ and f_D. ($x/D = 40$, $y/D = 0$). The centreline for the passage of the dislocations is defined by $z^*/D = 0$.)

The transverse profiles of fluctuation energy in figure 16 at $x/D = 20$, show that the central dominating energy peak is directly attributable to the dislocation frequency f_D, while the two side humps in the total energy are caused by the remaining energy at f_R (hence the shape of the total energy profile comprises a central peak with side humps).

Relevant to these fluctuation energy profiles, it can be seen that not all of the total energy at, for example, $x/D = 40$ in figure 15 is represented only by f_D and $2f_D$, because there are other harmonics contributing to the total (non-sinusoidal) waveform representation. An alternative means to determine the energy at f_D harmonics is to ensemble average the velocity signals at the frequency f_D, thus excluding any components at f and f_R. The resulting fluctuation profile has been included in figure 40 of Appendix B, where we can see that the total energy is almost wholly accounted for by the energy at all the f_D harmonics.

Finally, the plots in figure 17 show the decay of the energy as the flow progresses downstream. This total integrated energy E is defined by

$$E = \int_{-\infty}^{\infty} \left(\frac{u'_{\mathrm{rms}}}{U_\infty}\right)^2 \mathrm{d}\left(\frac{y}{D}\right).$$

The integrated energy of a normal laminar wake has a rapid exponential decay, whereas the wake with dislocations shows a much slower decay, exhibiting a plateau between $x/D = 40$ and 80, and with an energy level that is at least an order of

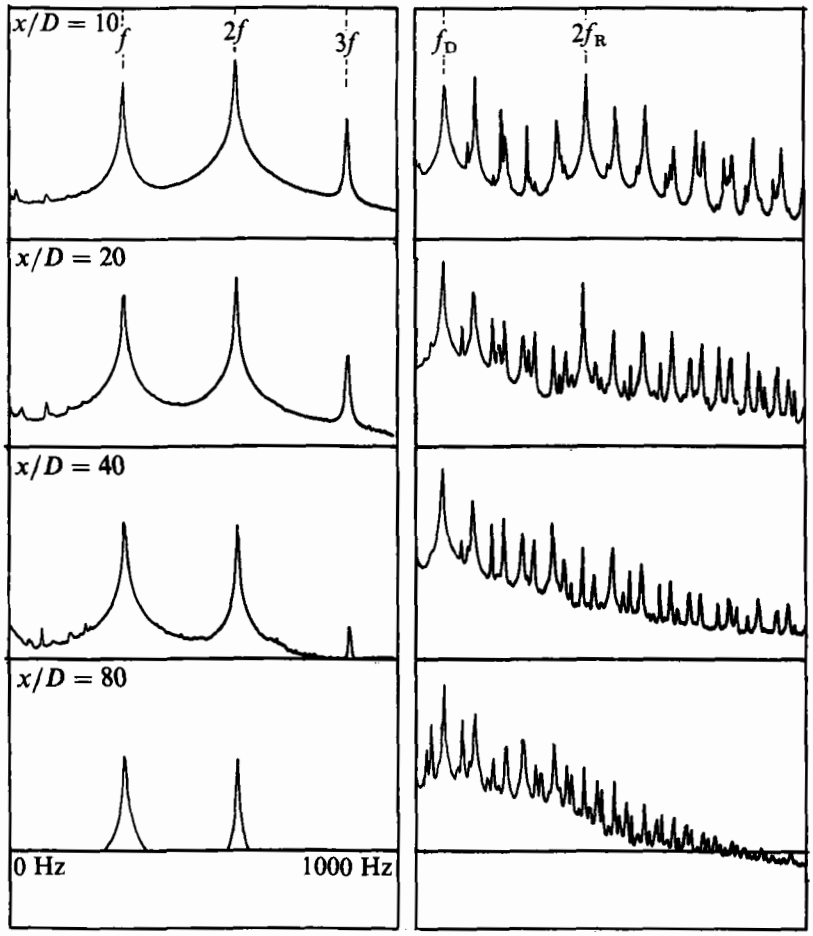

FIGURE 14. Spectra at different downstream locations. These spectra demonstrate the rapid (exponential) decay of fluctuation energy for a laminar street wake on the left which contrasts with the much slower decay of energy for the wake with dislocations on the right. It also demonstrates that near the ring disturbance the fluctuations are primarily at frequencies f_D and $2f_R$ (the probe is at $y/D = 0$, and $z^*/D = 1$, which is near to the centreline of the convecting dislocations). Downstream, the fluctuations at f_D and its harmonics easily dominate the other frequencies.

magnitude greater than that for a normal wake (see figure 35). Again, by looking at the components of this integrated energy at the different frequencies, it can be seen in figure 17 that the dislocation energy is almost wholly responsible for the plateau.

5.3. *Comparison with velocity measurements for one-sided dislocations*

At this point it is worth comparing the general features of the fluctuation profiles for a two-sided symmetric dislocation with the results for a one-sided dislocation shown in Gerich (1986), where he made measurements in the region near the end of a cylinder span. In this region, Gerich showed that there exists an end cell of low frequency, which interacts with the frequency of the rest of the span, and therefore we can expect periodic one-sided dislocations to occur (as observed in figure 7). Both the one-sided dislocations and also the present two-sided dislocations cause maxima in the spanwise fluctuation profiles. In the transverse profile, we again find, for the

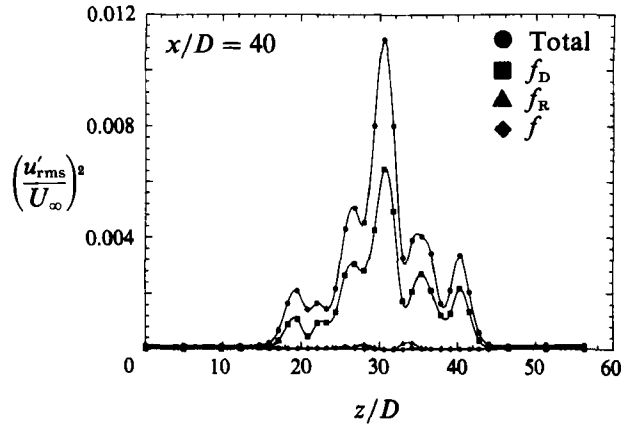

FIGURE 15. Energy at different frequencies (spanwise). These profiles of fluctuation energy show how the energy at different frequencies is distributed (spanwise) across the dislocations, and it is shown that the humps in the fluctuation profile are all due to the low-frequency dislocation structure ($y/D = 0$).

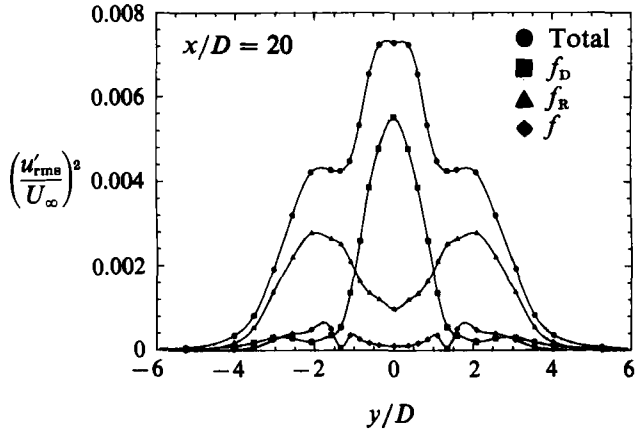

FIGURE 16. Energy at different frequencies (transverse). The profiles of fluctuation energy at different frequencies demonstrate clearly that the central large peak in the total energy profile at $x/D = 20$ is caused by the passage of the dislocations, whereas the two side peaks are caused by the two rows of vortex structures (in a vortex street configuration) that are shed behind the ring disturbance.

one-sided dislocation, a central dominating peak due to the evolving large structures, and the two side humps from the two rows of smaller shedding vortices.

Vortex-reconnection regions (or one-sided dislocations) are also present in the investigation of Lewis & Gharib (1992) for the wake behind a stepped cylinder (a cylinder with different diameters over each half span). In this case, two different shedding frequencies interact near the step-change in diameter. The spanwise profiles of both mean and fluctuation velocities are qualitatively similar to those found here, particularly when one compares their plots with only one side of the profiles for a two-sided dislocation. We can conclude from these comparisons that the types of large-scale fluctuation that are demonstrated for a two-sided dislocation are also found for a one-sided dislocation in a rather similar fashion.

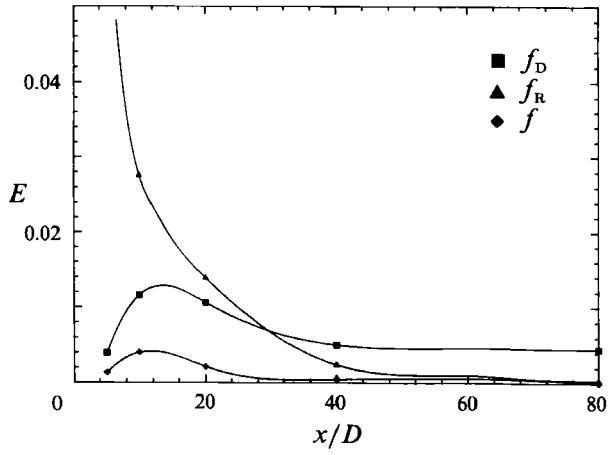

FIGURE 17. Downstream decay of integrated energy. The decay of integrated energy (across the transverse fluctuation profiles) for the laminar street wake follows very closely a rapid exponential decay, whereas the wake with dislocations exhibits a plateau region where the fluctuations decay very slowly with downstream distance. In the above figure, the contribution to the total energy from each of the frequencies shows that the plateau is due to the dislocation energy itself.

6. Aspects of vortex dynamics in a dislocation

6.1. *Downstream development of vortex dislocations*

The streamwise extent of a vortex dislocation is dependent on the diameter of the ring disturbance (D_R) relative to the cylinder diameter (D), and a simple analysis can show that the ratio of the wavelength of the dislocation (λ_D) to the primary vortex shedding wavelength (λ) varies roughly like

$$\left(\frac{\lambda_D}{\lambda}\right) = \left(\frac{D_R/D}{D_R/D - 1}\right).$$

It is to be expected that the dislocation frequency will decrease as the ring diameter decreases, as shown in the measurements of Appendix A, and correspondingly the wavelength of the dislocation will increase.

In figure 18, we can see the downstream development of a rather massive dislocation (from a ring disturbance of $D_R/D = 1.1$) with a streamwise wavelength of around 14 primary wavelengths, or a distance of about 75 diameters. The spanwise extent of the dislocation, when it is 100 diameters downstream, is around 8 primary wavelengths or 45 diameters. The size of these structures can be compared with those smaller dislocations (induced by larger ring disturbances) shown earlier in figures 6–8. It can also be seen from figure 18 that the dislocation is still spreading out laterally for about the first 100–150 diameters at least. Also in the figure, there is a region where the vortices across the dislocation are nearly in phase, with another region where they are predominantly out of phase, and where vortex division occurs.

A close detailed view of the divided vortices in a dislocation is given by the two-colour stereoscopic visualization sequence of figure 19(*a*)–(*f*) (plates 2 and 3). (In order to visualize three-dimensionalities from these stereoscopic pairs of images one can purchase a special inexpensive viewer, or use the 'cross-eyed' approach, both of which are discussed in Appendix B. The intent with stereoscopy is that each eye sees a separate image, and the brain fuses these images into a single three-dimensional

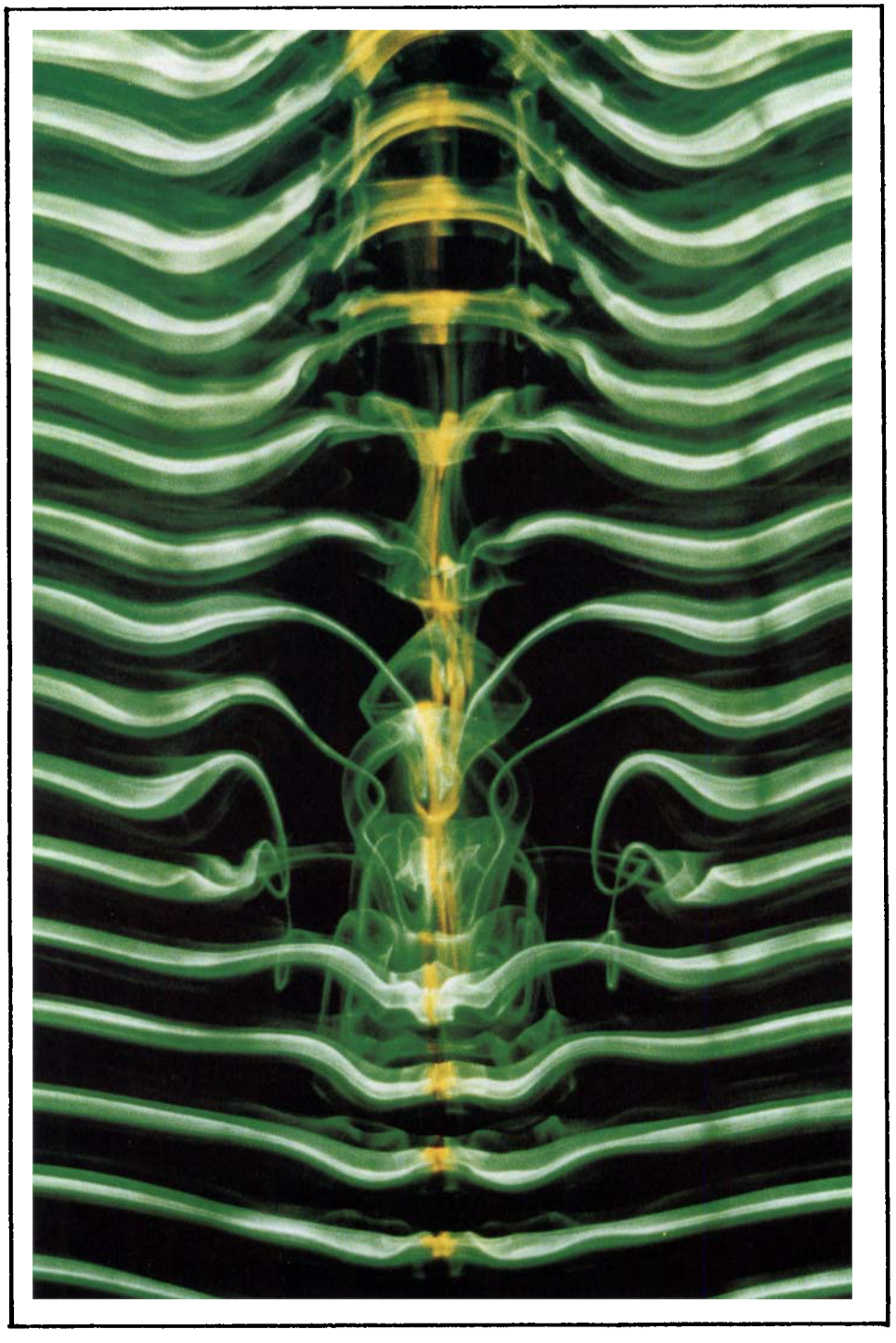

FIGURE 20. Overall colour visualization of a vortex dislocation. In this visualization we can see that the spanwise extent of the symmetric dislocation is far larger than the width of the ring-disturbance wake (shown as the yellow dye). It can also be seen that the structures can be remarkably symmetric either side of the ring disturbance, including similar detailed vortex linking and 'wisps' of stretched vortex tubes. The position of the upstream edge of the dislocation is around $x/D=22$.

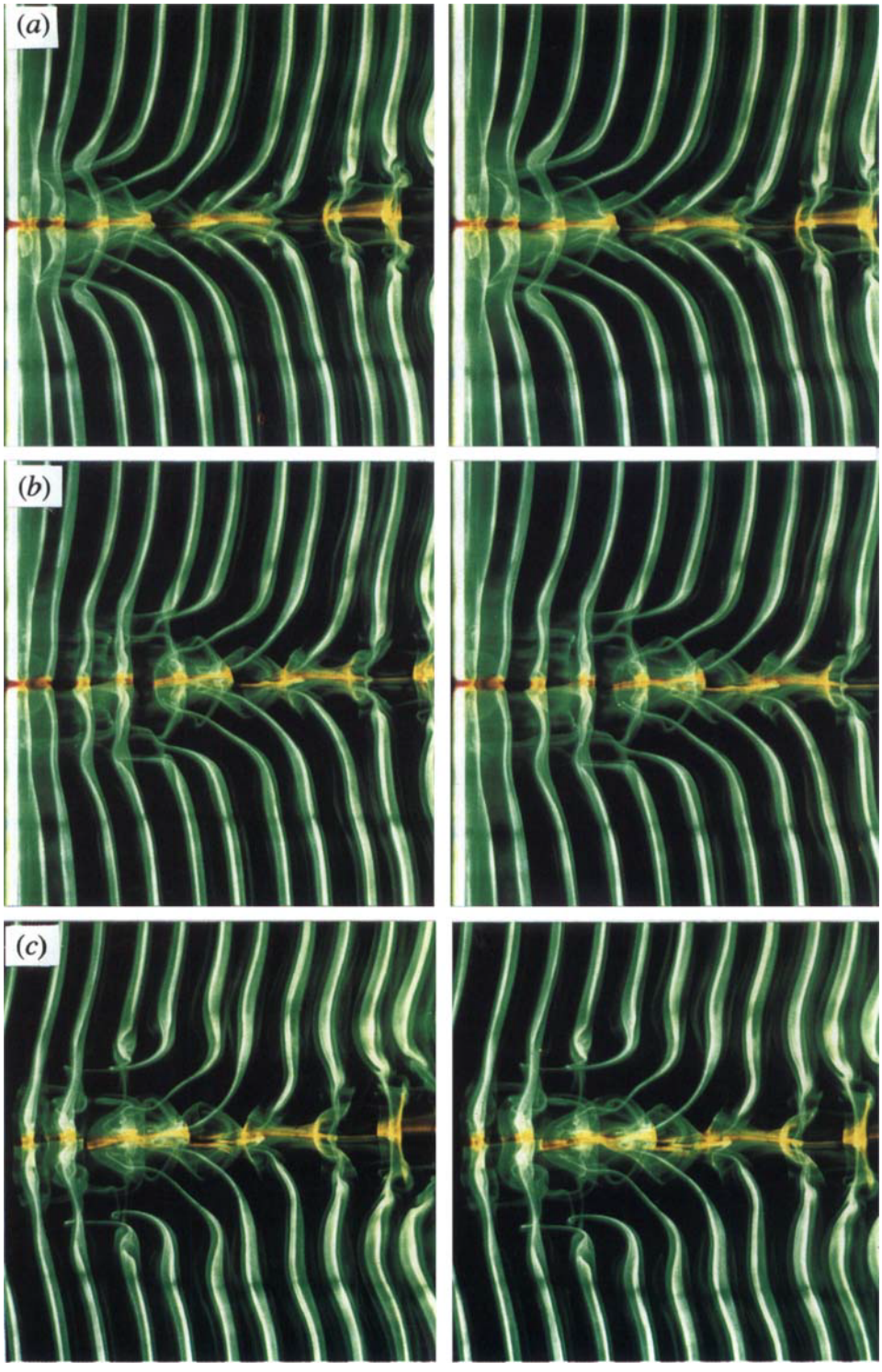

FIGURE 19. Colour stereoscopic visualization of the evolution of a symmetric dislocation. This stereoscopic sequence demonstrates the very complex three-dimensional nature of dislocations, which may be viewed in three dimensions following the techniques described in Appendix B. The intent is that each eye should view

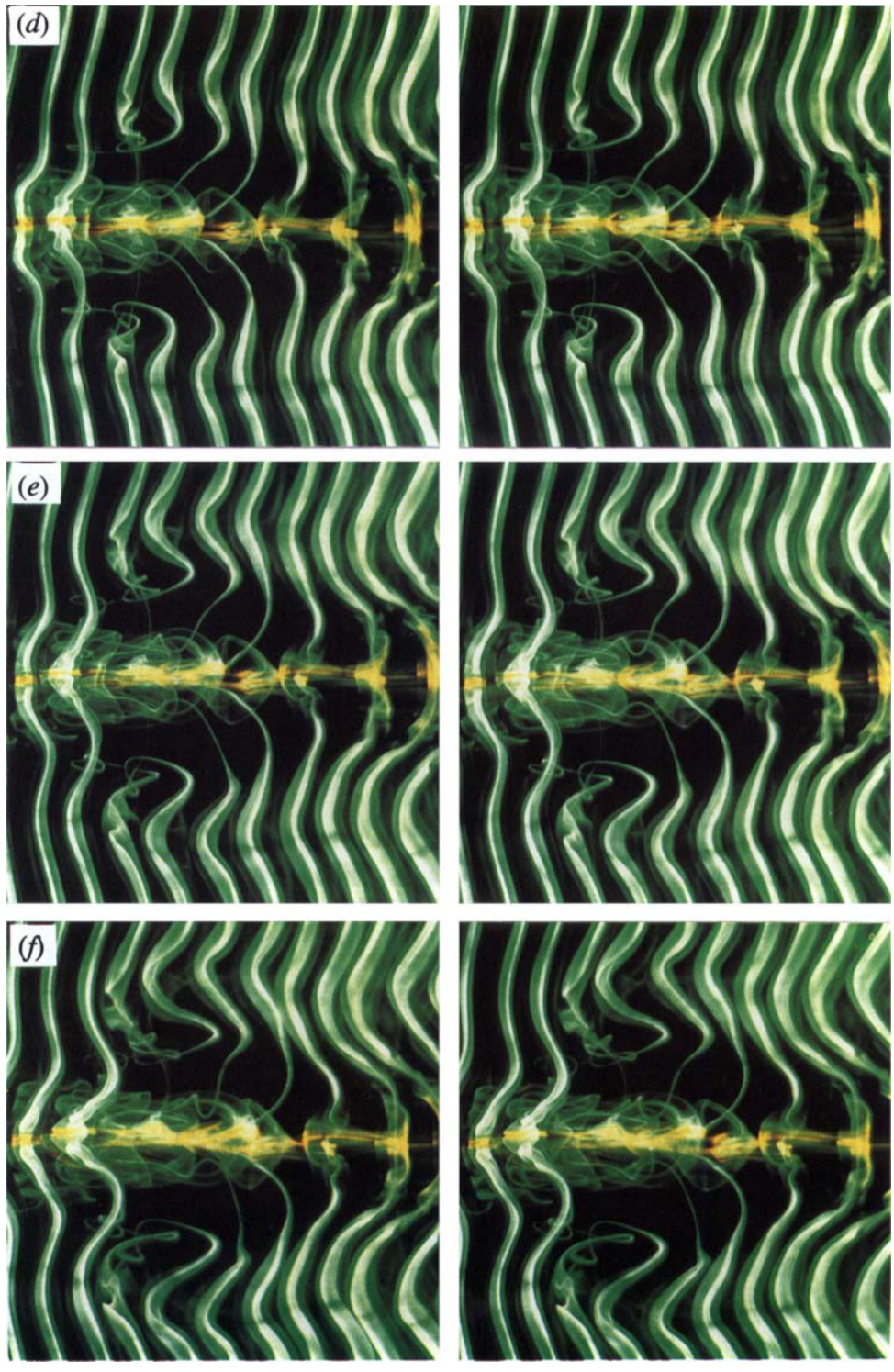

a separate image, which the brain fuses together. Particularly noticeable are the stretched streamwise vortex tubes in the dislocation, which become long 'wisps' that are wound around other vortices. The position of the upstream edge of the dislocation region is given by x/D values of: (*a*) 5; (*b*) 10; (*c*) 15; (*d*) 20; (*e*) 25; (*f*) 30.

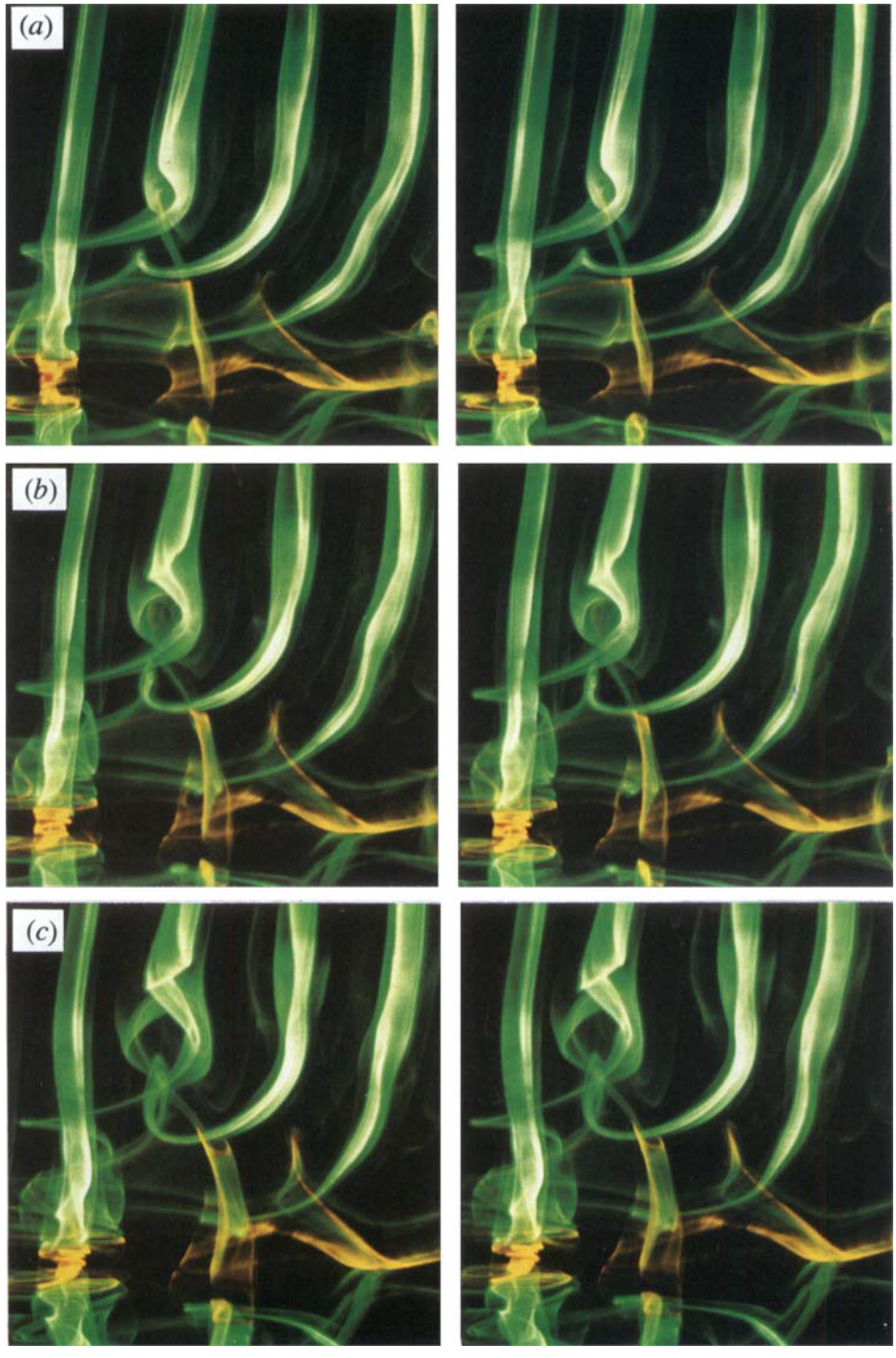

FIGURE 24. Colour stereoscopic visualization of spanwise spreading of a dislocation, by helical twisting of vortex tubes. This sequence shows the development of helical twisting of vortex branches, which leads to axial core flow in the vortices. This is a fundamental cause of the rapid spanwise spreading of dislocations, and indeed for the large-scale distortion and break-up to turbulence in a natural transition wake.

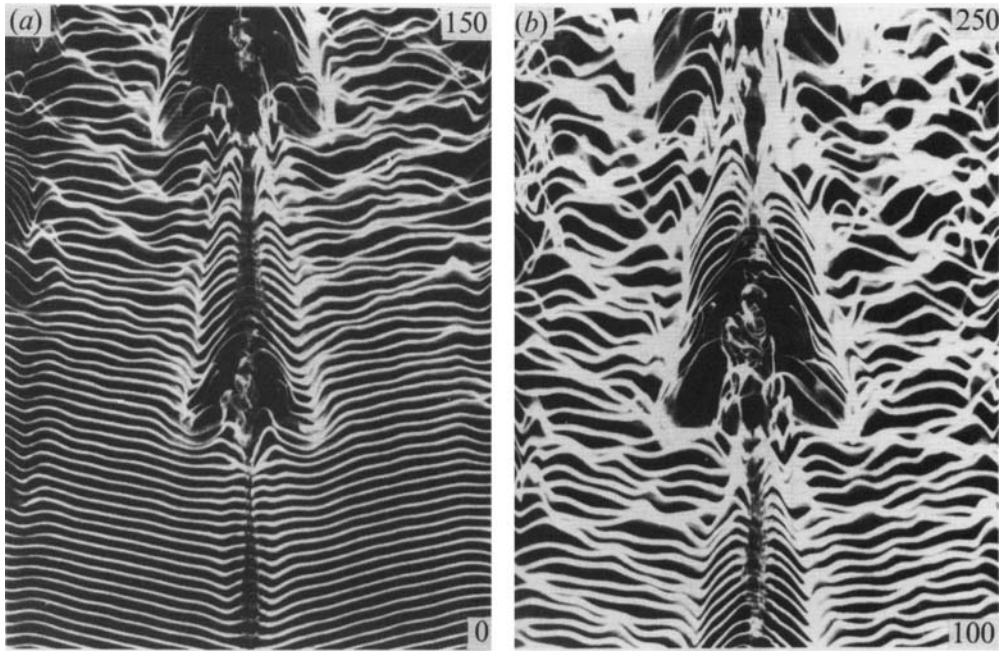

FIGURE 18. Spanwise development of a large-scale symmetric dislocation. The main features of a dislocation can be seen in this visualization of a rather massive structure induced by a small ring disturbance ($D_R/D = 1.1$). Some idea of the size is given by the numbers in the margins, showing values of x/D. The two photographs show the same A-structure at different times (or downstream distance). Flow is upwards.

structure.) In figure 19, the orange dye marks only the vorticity shed from the ring disturbance, while the green dye is that vorticity shed from the remaining cylinder. The use of two colours in this context is an idea that was triggered from the work of Gad-el-Hak *et al.* (1981). They marked the wake of a surface obstacle that was used to trigger turbulent spots in an otherwise laminar boundary layer, by a colour that was different from that in the surrounding fluid. They found that the spot spread laterally much further than the actual wake of the obstacle itself, and concluded that the spanwise 'contamination' mechanism is related to a laterally propagating instability that was termed 'growth by destabilisation'. In the present case also, the spanwise propagation of the dislocation takes place without necessarily the shed vorticity from the ring being directly involved. This spreading mechanism is further discussed in §6.3 below.

The stereoscopic nature of the visualization yields a remarkably complex and rather beautiful three-dimensional structure, which is not seen clearly by a two-dimensional presentation. Associated with the vortex division and the bent vortices at the sides of the dislocation, is an axial core flow outward along the vortices. This axial flow causes the vortex tubes to be stretched into wisps within the dislocation, while those parts of the tubes situated on the outskirts of the dislocation are fattened. It should also be mentioned that the vortices at the edge of a dislocation do not tend to bend over 180° and become attached to vortices of opposite sign, which would clearly be a tempting conclusion, based solely from later photographs in the sequence. By looking earlier in the sequence one can observe that this is not the case. Lastly, to provide an overall close-up perspective of the dislocation

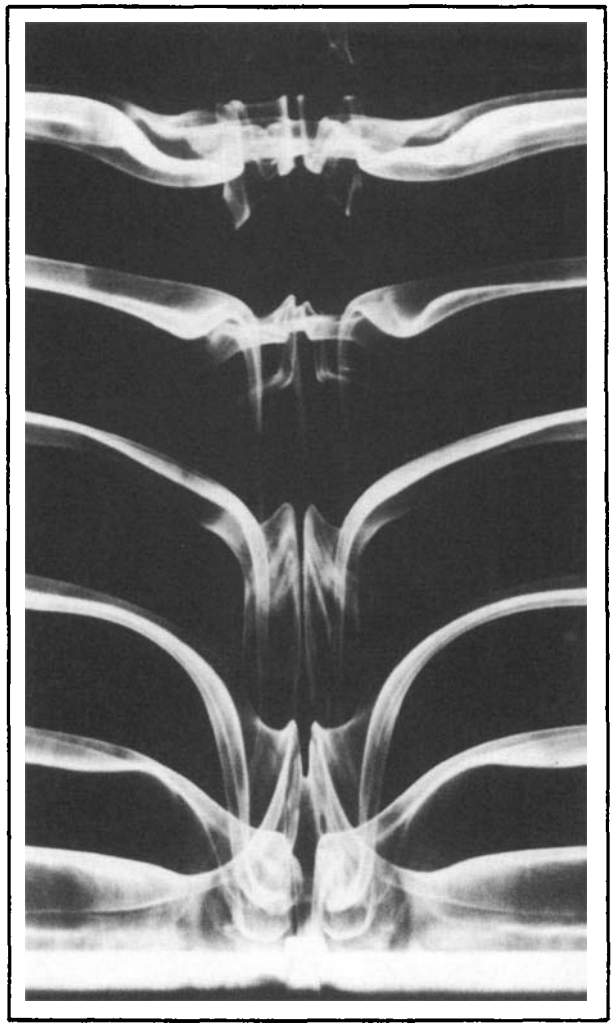

FIGURE 21. Close-up visualization of vortex formation near the ring disturbance. This photograph demonstrates that the near-wake vortex interaction is by no means simple. Such visualization shows that the vortices can divide (or branch) into two other vortices of the same sign.

described above, a colour photograph of a two-sided symmetric dislocation is shown in figure 20 (plate 1), where the large size of the overall dislocation is evident in comparison with the (orange) wake of the ring disturbance.

6.2. *Vortex linking across a dislocation*

The large-scale visualization in figure 21 suggests a type of linking whereby a vortex of one sign is divided and typically linked to two vortices of the same sign on the other side of the cell boundary. This was observed also for the one-sided dislocation shown in figure 23 of Williamson (1989*a*). A diagram of the primary vortex linking across a dislocation based on the type of linking that can be seen between the first and third vortex from the bottom of the photograph, is shown in figure 22(*a*). Only the central cores of the vortices are represented by the lines, and we do not include

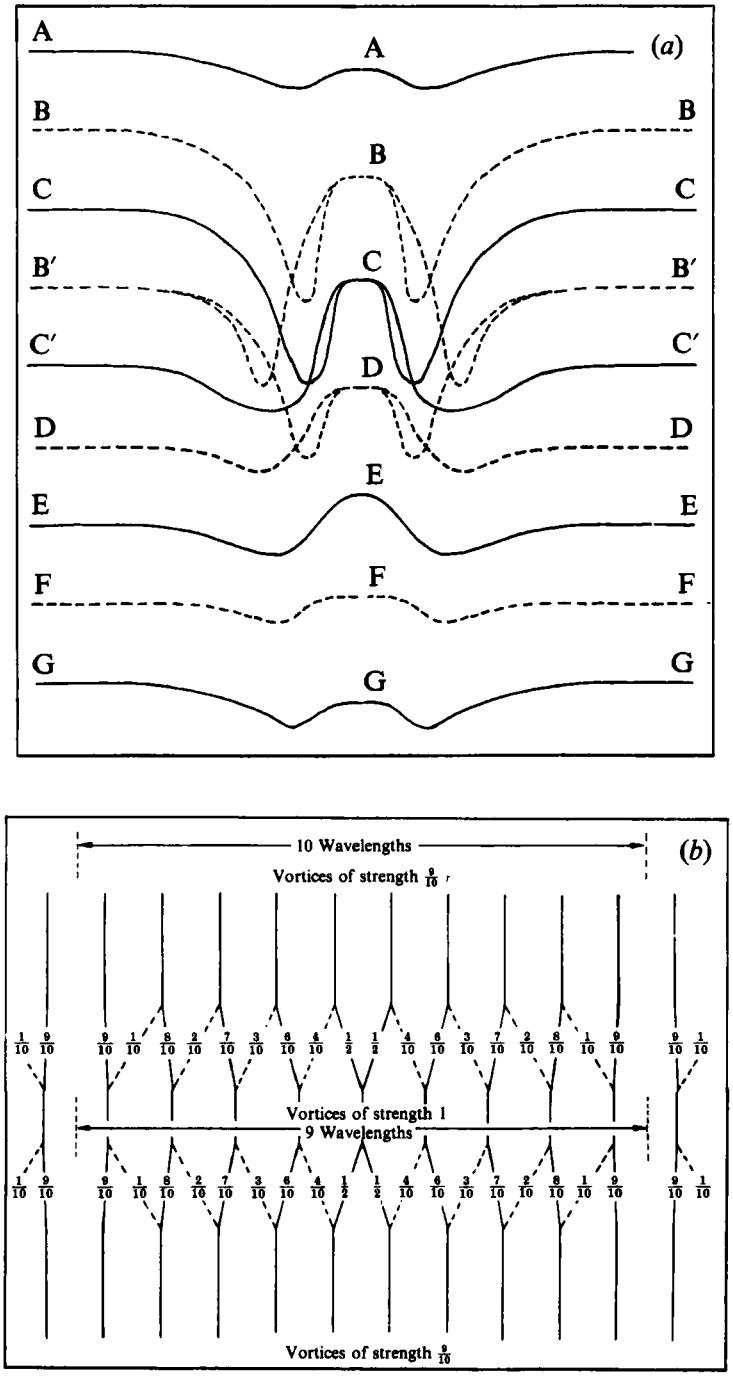

FIGURE 22. Vortex linking across a two-sided dislocation. In (*a*), only the primary vortex links (inferred from visualization such as figure 21) are shown. It can be seen that vortices can divide (or branch) into two vortices of the same sign in a neighbouring cell. In (*b*), an idealized sketch is drawn of the vortex links across a dislocation that is moving to the right. The strengths of the vortex links are given by the numbers.

other possible linking that will occur for the outer vortex sheets of the rolled-up vortices. Such outer vortex sheets are clearly difficult to see owing to their stretching and diffusion. Hence, in the diagram not all the vortices have the complex linking shown for vortices B, C and D. It can be seen that vortex B in the centre is attached to both vortex B and also B′ on each side. Similarly, C is attached to C and C′, and so on. Parts of the links are stretched into vortex loops in the streamwise (vertical) direction, because the loop ends get left behind near the body as the vortices travel downstream. This can be seen in figure 19 between (*a*) and (*b*), also in figure 21, and is simply represented in figure 22(*a*) as the downward-pointing loops.

Based on the above observations, an idealization of the vortex links is schematically drawn in figure 22(*b*), in which figure we make the assumption that there are 10 wavelengths either side of the dislocation (upper and lower parts of the figure) to every 9 wavelengths within the dislocation (central part). An assumption is made, based on the earlier discussion, that all the vorticity of one cell is connected to the vortices in the other cell, rather than turning around 180° and being linked to other vortices of the same cell. Figure 22(*b*) shows the relative strengths of the vortex links (indicated by the numbers) between the outer cells and the inner cell. It is assumed that the cells convect downstream (to the right) at the same speed, and that circulation is produced at the same rate upstream for each cell. (The latter is a reasonable assumption given that the rate of circulation production from each side of the body approximately depends on the free-stream velocity, and not the diameter). If we suppose that the central vortices are of unity strength, then the outer cell vortices will have a strength 9/10. Obviously the relative phase of the inner–outer cells affects the picture, and this sketch shows only one possibility. The starting point in drawing the figure was the supposition that a central vortex (1) divides into two halves. Then vortex (2) in the upper cell will divide into vortices of strength 1/2 and 4/10. Vortex (3) in the central cell will then divide into vortices of strength 6/10 and 4/10, and so on, until the complete sketch is built up. What is of interest in this idealization is the relative strength of the vortex links. It is quite possible that the weaker links (say 3/10 strength or below) will be difficult to see in an actual experiment, especially as they may involve vorticity more spread out in the outer layers of the vortices, rather than the more obvious rolled-up core regions of the vortices, as discussed above. It may therefore be difficult to trace, in an experiment, all of the vortex linking that might be suggested from such an idealized model.

6.3. *Mechanism of spanwise spreading and 'climbing' of dislocations: dynamics of divided vortices, and axial core flows*

We can measure the rate at which a dislocation spreads into the surrounding street vortex pattern by measuring the half-angle between a line that joins the outer edges of a sequence of dislocations and a line that points downstream. In the present case, this 'visual' spreading angle α, presented in figure 23, is measured taking into account the first three dislocations downstream of the body. It is shown to increase with Reynolds number, reaching an asymptote close to 12°. A different spreading angle can also be given by the mean and fluctuation profiles, in which case the spanwise extent of the dislocation is taken to be the distance between the two velocity minima either side of the dislocation, as shown, for example, in figure 10. Again, the values of α tend to asymptotes near 12° for the U-profiles, and near 18° for the $u'_{\rm rms}$ profiles. Overall, the dislocations are found to spread surprisingly rapidly as they travel downstream. It should also be pointed out that the visual spreading

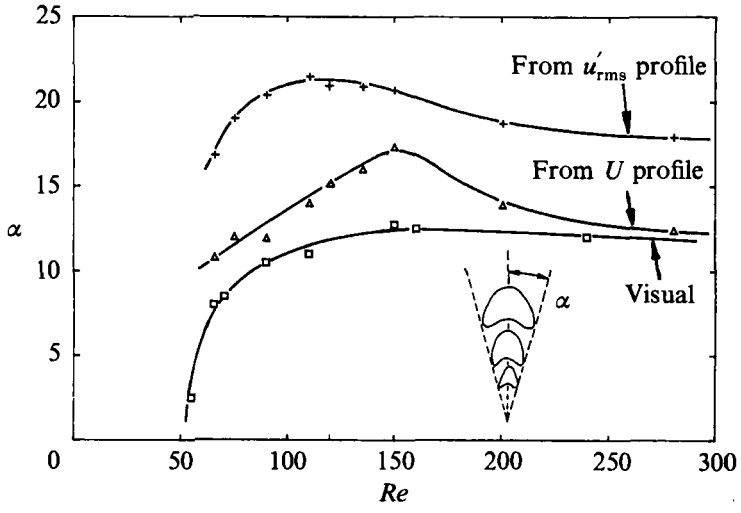

FIGURE 23. Spanwise spreading angles of dislocations as a function of Reynolds numbers. Measurements of the spreading half-angle are shown from visualizations (□), and are also extracted from mean velocity profiles (△), and from fluctuation profiles (+).

angles are numerically similar to those for boundary-layer spots as found, for example, by Schubauer & Klebanoff (1956).

From the measurements of visual spreading angle, the axial velocity of the spanwise edges of the dislocation can be deduced. In solid crystal dislocation and in the studies of Browand *et al.* (1991) for a shear layer, this type of spreading motion has been termed 'climb'. An expression for the axial 'climb' for the present case can be given as

$$U_A/U_\infty = (U_C/U_\infty)\tan\alpha,$$

where U_A is the axial climb velocity, and U_C is the downstream convection speed of the structures. We can estimate U_C/U_∞ to be 0.9, and the half-angle α to be 12°, giving a rather rapid axial climb velocity of

$$U_A/U_\infty \sim 0.20.$$

In order to investigate the vortex dynamics that are responsible for the high rate of axial climb (or spanwise) spreading, a further two-colour stereoscopic visualization sequence is shown in figure 24 (plate 4). This figure shows a close-up of the vortex division at the outer spanwise edge of a dislocation (that is moving downstream to the right). The divided vortex of interest here is the green one that is second from the left. The two distinct divided branches of the vortex are observed to 'unravel' helically from the originally single vortex tube, causing an upward axial flow or induced velocity.

In order to understand the axial motion of these helical vortex branches, one can consider the example of a hollow vortex composed of several vortex tubes which are, for simplicity, all situated on an outer cylindrical surface parallel to a central axis. If these tubes are parallel to the overall vortex axis, then the induced velocity will be solely around the axis of the vortex (circumferential). If, however, the vortex tubes are situated each on a helix on the outer cylindrical surface, then there will be axial as well as circumferential flow velocity components in the vortex core. A computation which illustrates this type of configuration was made by Leonard (1985) in his figure 11. The core flow direction corresponds with the right-hand thumbscrew

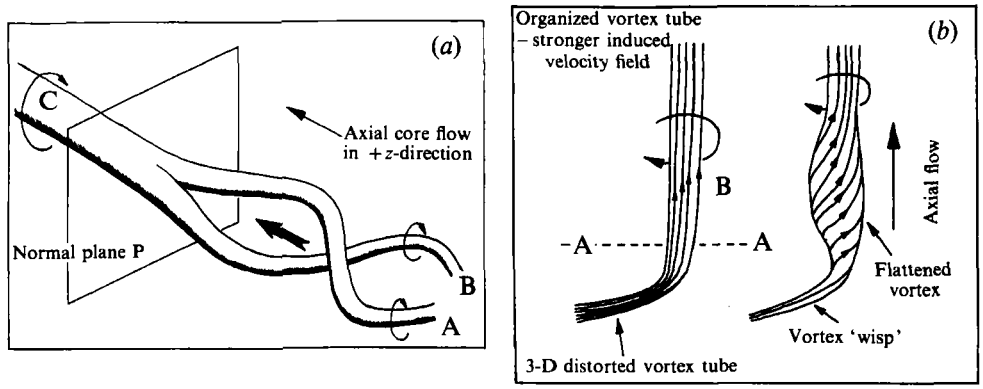

FIGURE 25. Mechanism for spanwise spreading: helical twisting of vortex tubes and axial core flow. (*a*). A mechanism is shown whereby vortex branching leads to an outward axial flow. The rotation of vortex tube C tends to helically rotate vortex branches A and B about each other, resulting in a component of axial flow towards C. (*b*) A mechanism is sketched whereby a vortex tube with spanwise non-uniformity can cause axial flow, by helical twisting of vortex lines.

rule as shown in figure 25(*a*). If the vortex branches are clockwise rotation (+) into the page, then the helix will be clockwise rotation (+) into the page, because the unravelled part of the main vortex (on the other side of the page) will twist those branches in close proximity. The resulting axial flow is also into the page (+). If we put this algebraically,

(sign of the axial flow direction) = (sign of vorticity) (sign of helix) = positive.

On the other hand, if the vortex branches are spinning anticlockwise (−), then the helix will be anticlockwise (−) into the page, and the axial flow will be (−)(−) = (+), i.e. again into the page. Thus vortex branching on both (transverse) sides of the wake will spread outwards from the dislocation. In the present case, we have two helical vortex branches shown as A and B in the schematic of figure 25(*a*), which similarly produce an axial flow along the vortex. The main vortex element C in plane P is induced to further split itself into two branches, because of the strain rate field due to the vortex branches.

A related mechanism for spanwise outward axial flow occurs for the vortices at the edge of the dislocation that are bent into the streamwise direction, as shown for example by the third green vortex from the left in figure 24. There is an upward axial flow which causes the (lower) streamwise vortex 'wisps' to become thinner, while the upper parts of the vortex tubes become fatter. If we look at the diagram in figure 25(*b*), it can be seen that the induced rotation on a vortex element (near B) due to the organized vorticity above section AA will be stronger than the more-distorted and re-oriented vorticity below AA (within the dislocation). The vortex lines will tend to twist, resulting in helical vortex lines and an axial flow upwards. The fattened part of the vortex will have a higher pressure than is found further up the vortex tube, and this pressure gradient will further drive the upward axial flow. This has some similarity with the theoretical ideas and computations of Lundgren & Ashurst (1989), who find that an axial pressure gradient in a vortex can cause a propagating wave of area and of axial velocity to move fluid from fatter to thinner segments of the vortex tube.

In summary, the twisting of vortex lines or vortex branches into helices at the edges of a dislocation leads to an outward axial flow. It is suggested here that this

is the primary mechanism for lateral spread or 'climb' of a dislocation. Such a mechanism also has significance during natural three-dimensional transition.

7. Overall Λ-structure of a symmetric two-sided dislocation: phase-locked measurements

7.1. *Phase-locked velocity fluctuations and velocity profiles*

In flows where there is forced or triggered periodicity, it is convenient to make measurements with respect to a reference signal of fixed phase relative to the large periodic structures. In the present case, one hot-wire probe is located downstream as a phase reference for the passage of large dislocations, while a second wire is traversed to different locations. 'Raw' waveforms are ensemble averaged at the dislocation frequency f_D over 200 dislocation cycles to yield purely cyclic fluctuations.

From phase-locked velocity signals for $x/D = 40$, $y/D = 0$, we can assemble 'instantaneous' velocity profiles for particular phases during the downstream passage of a dislocation. (Appendix C shows that most of the energy associated with dislocations at $x/D = 40$ is due to the dislocation waveform alone.) Spanwise 'instantaneous' profiles are found in figure 26(*a*), for values of the phase corresponding to certain physical positions on an actual dislocation indicated earlier as part of figure 8. Interestingly, the downstream velocity in the out-of-phase part of the dislocation for $t = 0$ is even found to exceed the free-stream velocity. Overall, these 'jet-like' instantaneous profiles are consistent with the observations that the vortices to each side of a dislocation travel upstream (in relative terms) thus causing the overall Λ-shaped structure. The transverse instantaneous profiles shown in figure 26(*b*) are again strongly dependent on position in the dislocation. The profile at $t^* = 3T/4$ is much like that for the classical street wake to either side, and corresponds with the part of the dislocation with in-phase vortices, whereas the profile for $t^* = 0$ is markedly different and corresponds with the downstream flow in the out-of-phase region.

7.2. *Velocity contour plots and overall Λ-structure*

Contours of equal fluctuation velocity are shown in figure 27(*a*) (plate 5), where red indicates upstream velocity (relative to the local mean velocity) and blue shows downstream velocity. Contours of equal total velocity (local mean plus local fluctuation velocities) are found in figure 27(*b*) (plate 5), where white is chosen as the velocity found in a normal street and red is again relative upstream velocity. In these plots, time has been normalized into a downstream coordinate using Taylor's hypothesis, and although not strictly correct, the plots may be used to approximately represent the instantaneous velocity contour levels in the centreplane of the wake.

There is immediately one rather satisfactory conclusion to be drawn from figure 27, and that is the remarkable symmetry either side of the dislocation, even to the level of repeating the small 'substructures' on each side. This confirms that the stable configuration for a two-sided dislocation is certainly a symmetric Λ-shaped structure. (During the time it took to complete these measurements, we can estimate that there must have been of the order of 500000 dislocation structures passing the probe, so one can assume that the pattern could continue indefinitely!) The red region of upstream flow in figure 27(*a*) indicates the induced velocity due to the in-phase vortices in their Λ-shaped configuration, as is shown diagrammatically in figure 29. The blue region is the more downstream velocity associated with the out-

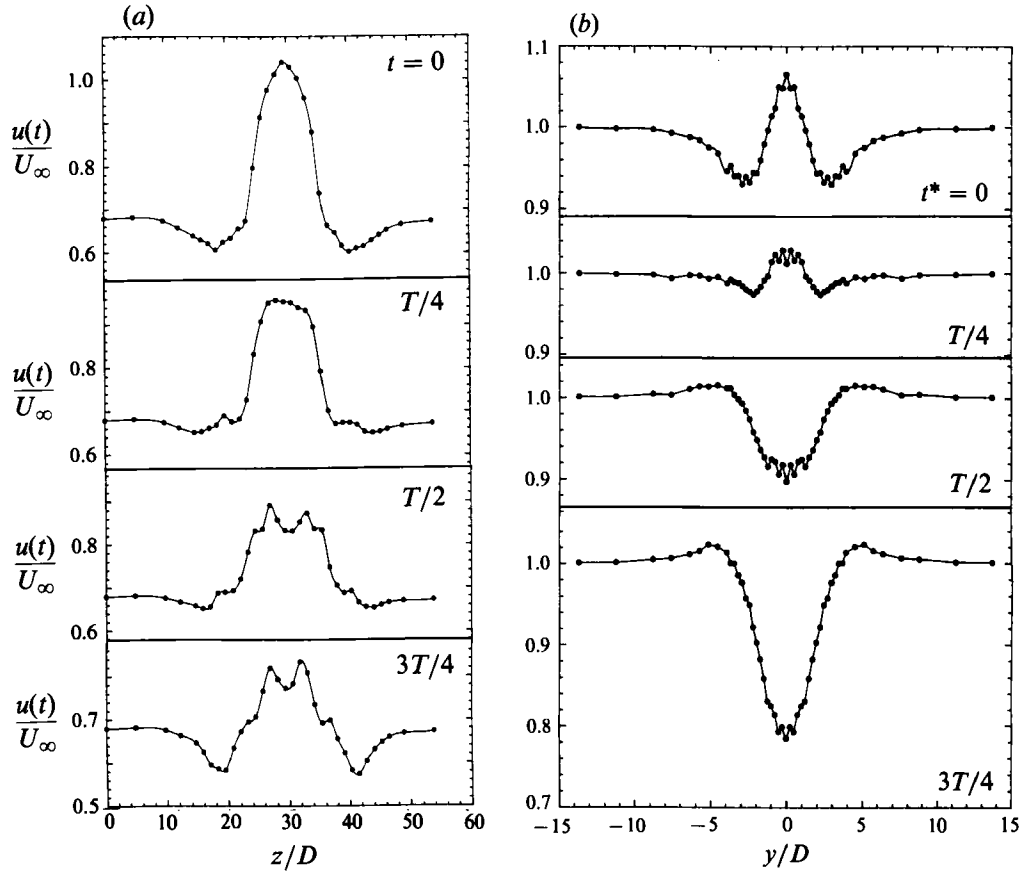

FIGURE 26. 'Instantaneous' velocity profiles. (*a*) Instantaneous velocity profiles (spanwise) are shown at different phases during the passage of a dislocation. These phases correspond with figure 8. A prominent feature to observe here is the jet-like effect due to the dislocation. (*b*) Instantaneous velocity profiles (transverse). These profiles show a radical change from the classical type of profile (as for $t^* = 3T/4$) usually found for vortex street wakes. There can exist a negative momentum defect in the centre of a profile. $x/D = 40$; $t^* = t - T/16$.

of-phase vortices. Similar contour plots are created in the transverse centreplane of the dislocation, as shown in figure 28 (plate 6), and again the red upstream flow is associated with the induced velocities in between the in-phase vortices at either (transverse) side of the wake.

Support for the downstream dislocation structure comprising a A-shaped vortex comes from smoke visualization in a wind tunnel shown in figure 30, with the smoke introduced far downstream at $x/D = 75$. The resulting smoke lines are predominantly distorted and wound around a pair of lines in a A-configuration. This result together with the contour plots above and the earlier visualizations indicates that indeed the overall structure comprises a pair of A-vortices which lie (almost like a mirror image) on either side of the wake centreplane, as sketched (in approximate form) in figure 31.

7.3. *'Substructures' in a A-shaped dislocation*

A certain waviness was found in the shape of the spanwise fluctuation profiles of figure 10, which suggests the existence of substructures within a dislocation. Figure

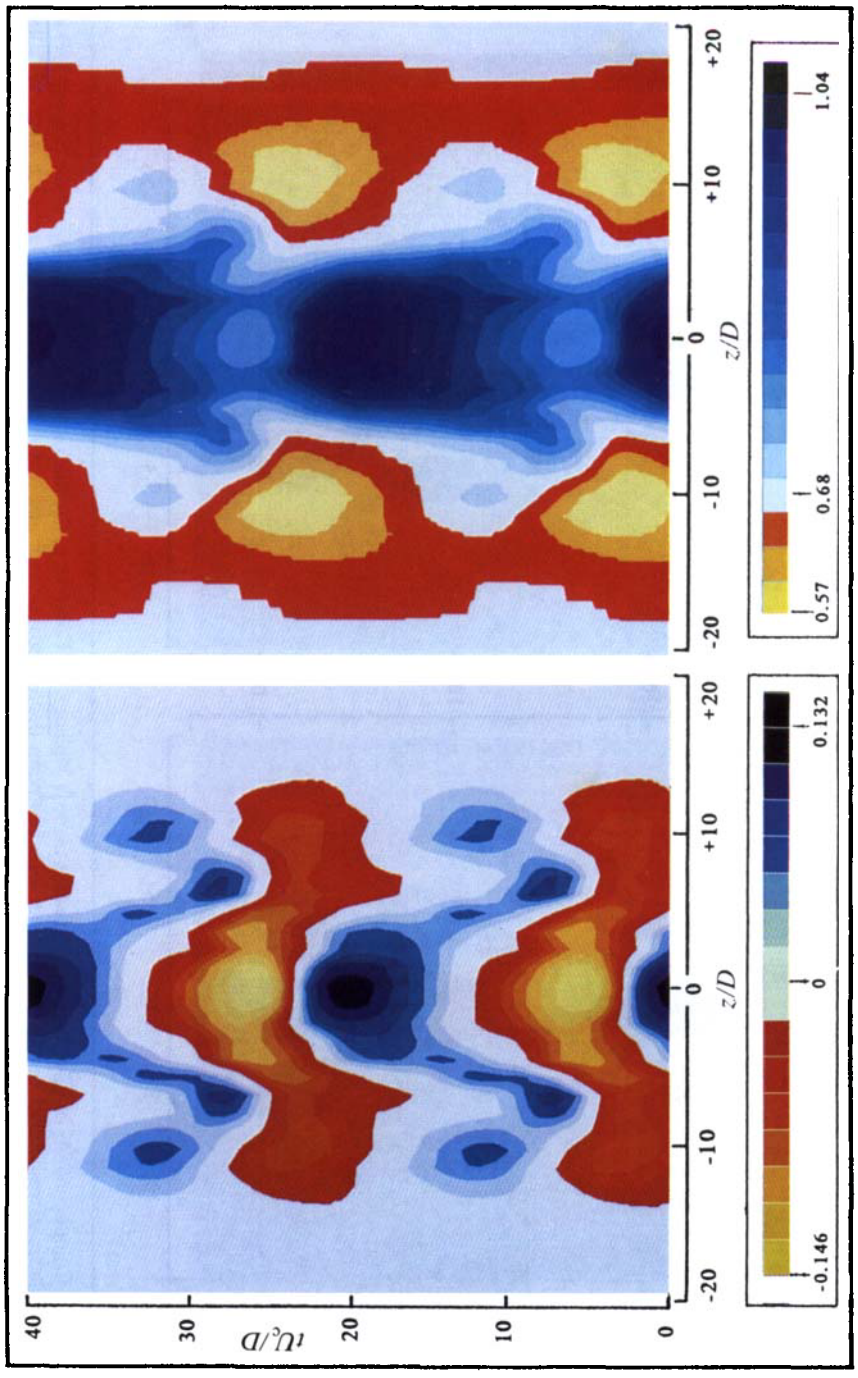

FIGURE 27. Colour contours of velocity in the spanwise plane (x,z-plane). (*a*) Contours of fluctuation velocity $\langle u'/U_\infty \rangle_{f_D}$ in the plane of z/D and tU_c/D. This proves that the stable configuration for a two-sided dislocation is symmetric (in phase). Upstream fluctuations are red, and downstream fluctuations are blue (steps of 0.0185). (*b*) Contours of velocity $\langle u/U_\infty \rangle_{f_D}$ again clearly demonstrating that the effect of dislocations is to push fluid downstream, relative to the induced upstream flow of a vortex street. The flow between the vortex street ($u/U_\infty = 0.68$) is assigned the white colour, with relative upstream flow as red, and relative downstream flow as blue (steps of 0.0315). $y/D = 0$, $x/D = 40$.

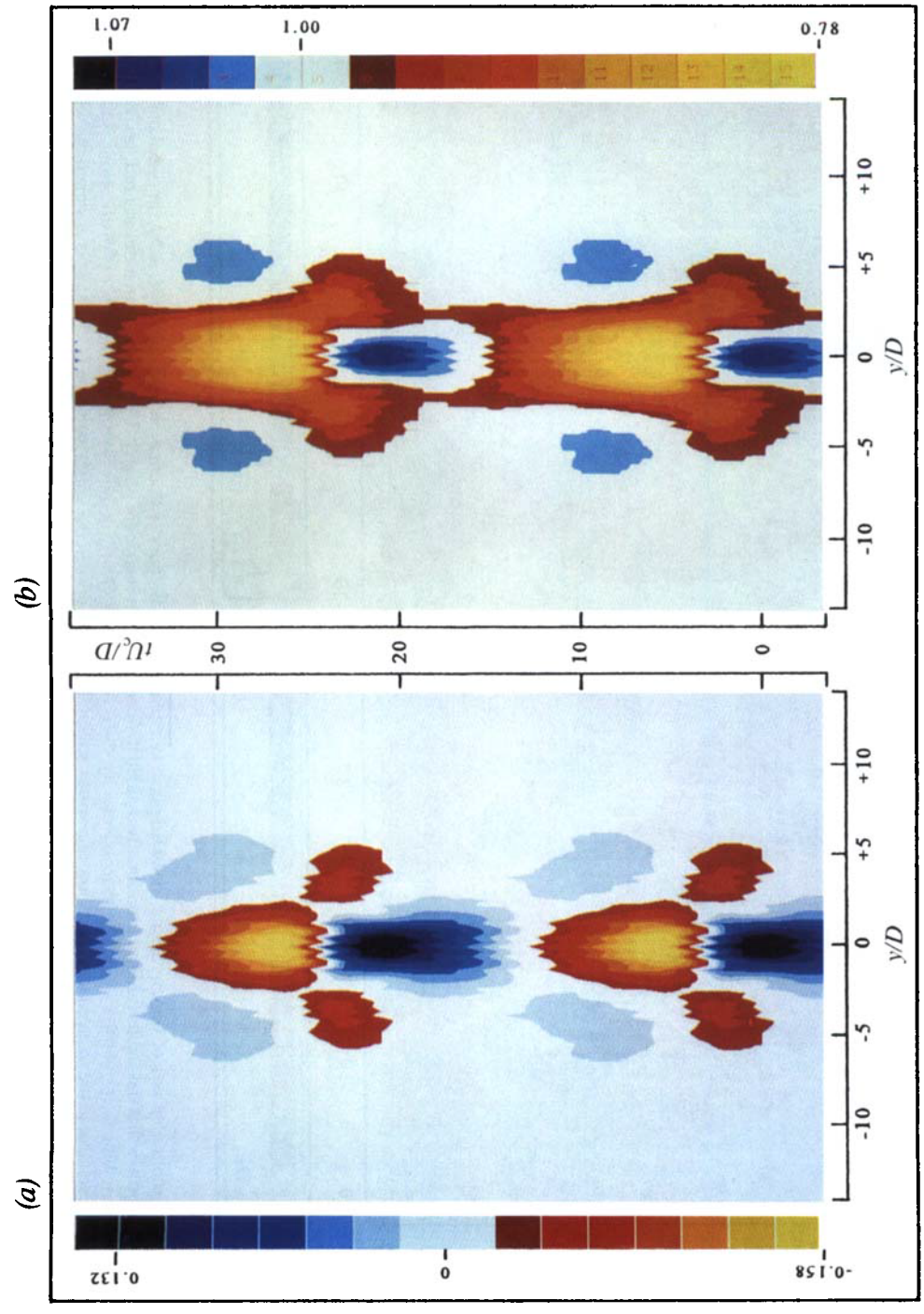

FIGURE 28. Colour contours of velocity in the transverse plane (x,y-plane). (*a*) Contours of fluctuation velocity $\langle u'/U_\infty \rangle_{f_D}$ in the plane of y/D and $\sqrt{2}U_c/D$, the latter corresponding approximately with x/D. Upstream fluctuations are red, and downstream fluctuations are blue (steps of 0.0181). (*b*) Contours of velocity $\langle u/U_\infty \rangle_{f_D}$. The flow outside the wake ($u/U_\infty = 1.0$) is assigned the white colour, with relative upstream flow as red, and relative downstream flow as blue. (Note that y/D negative is the image of measured y/D positive.) (Steps of 0.0179.)

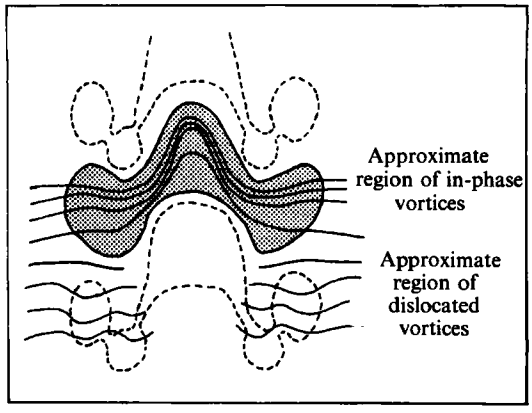

FIGURE 29. Relation between velocity contours and dislocation vortices. This indicates the position of the vortices relative to the contours of velocity fluctuation in figure 27. The in-phase vortices in a Λ-shaped configuration are responsible for the upstream flow in the spanwise centreplane (shown as red in the colour contour plot and as the shaded region above).

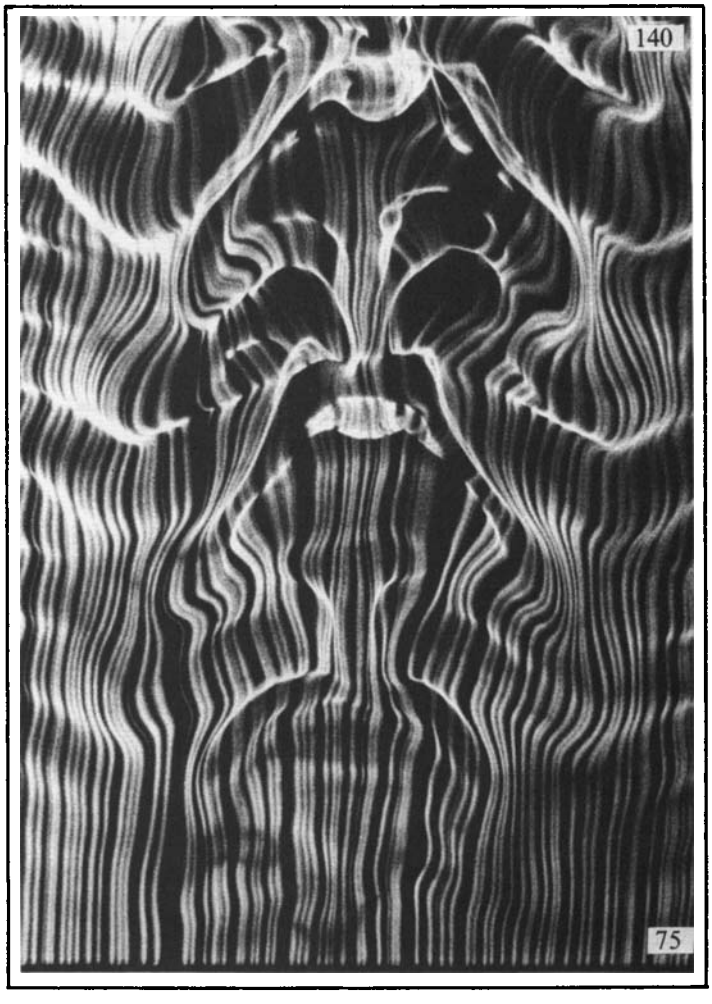

FIGURE 30. Λ-vortices visualized using smoke that is introduced far downstream. This visualization suggests that the principal feature of the two-sided (forced) symmetric dislocation is indeed a Λ-vortex, because the smoke, which is introduced far downstream (at $x/D = 75$), is immediately wound around two lines in a Λ-shaped configuration. (The numbers in the photograph refer to values of x/D).

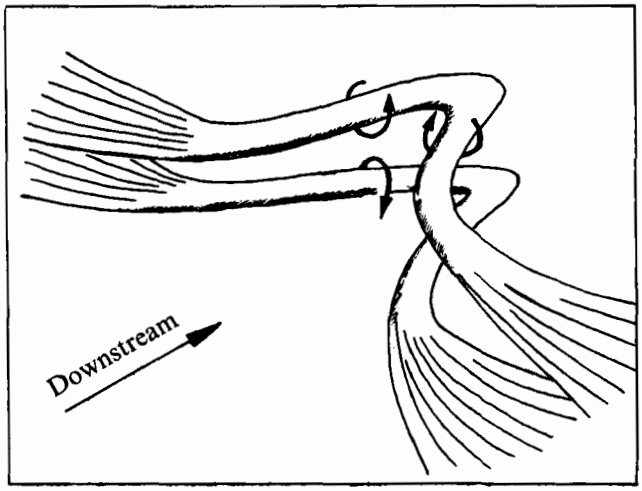

FIGURE 31. Schematic diagram of overall Λ-structure. It is suggested from the present results that the primary vortical structure of the symmetric two-sided dislocation in the far wake comprises a pair of Λ-vortices placed symmetrically with respect to the spanwise centreplane.

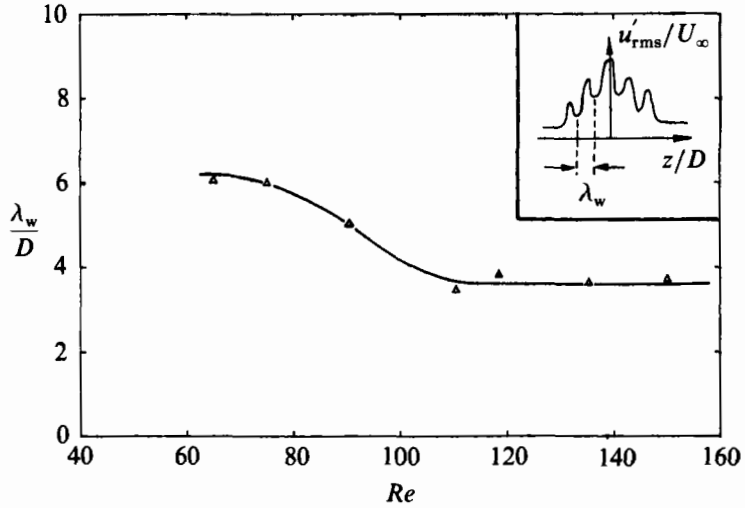

FIGURE 32. 'Substructure' spanwise wavelengths. These wavelengths are deduced from spanwise fluctuation profiles, as shown typically in figure 10. Substructure lengthscales are of the order of a primary wavelength ($5D$).

32 gives an indication of how the spanwise wavelength of these substructures varies with Reynolds number, taken from several fluctuation profiles, giving a wavelength of typically around one primary wavelength or $5D$. The fluctuation contours of figure 27 indicate that the substructures are caused by the out-of-phase vortices. It is suggested that these waves in the profiles are due to the helical waviness of the out-of-phase vortices, which would lead to spanwise fluctuations in velocity measured in the centreplane. This is consistent with visualizations which show a vortex waviness with a lengthscale of around one primary wavelength.

8. Discussion on vortex dislocations in other flows

In general, it is expected that a number of features of the present study will have similarities or counterparts with dislocations that may be found in other flows. There are a number of other flows that exhibit dislocations, such as the following:

(*a*) (non-uniform) shear flows past a cylindrical bluff body;
(*b*) flows past a non-uniform body geometry;
(*c*) free shear flows (spatially growing, as for flows from a splitter plate);
(*d*) free shear flows (temporally growing, as in 'tilting-tank' experiments);
(*e*) Rayleigh–Bénard convection patterns;
(*f*) flows over sand dunes and ripples;
(*g*) water ripple patterns;
(*h*) cloud condensation wave patterns;
(*i*) boundary-layer flows (possibly).

Features which one might expect to be similar for dislocations in many of these flows are, for example, the linking of wave fronts across a dislocation, the angles of the dislocation to the wave direction, the rapid spatial growth of dislocation regions, and the nonlinear interaction of the frequencies. In the case of non-uniform flows and shear flows, there are clear similarities, which are discussed below.

8.1. *Vortex dislocations in non-uniform flows*

Perhaps the most basic configurations of grossly non-uniform flows past bodies can be distilled into the following three types of flow. First, there is the shear flow past a cylinder (Maull & Young 1973; Griffin 1988), where different spanwise-frequency cells are found. Secondly, there is the uniform flow past a tapered cylinder or cone (originally studied by Gaster 1969, 1971, and now recently receiving attention from Picirillo & Van Atta 1991, and from A. Papangelou & M. Gaster 1991, personal communication). Thirdly, there is the stepped-cylinder study of Lewis & Gharib (1991), which is a rather convenient configuration for the study of frequency interactions. In all of these studies, the common physical feature is the development of what is defined here as a 'one-sided' dislocation. The line joining divided vortices in a dislocation is normally angled relative to the flow direction, which is consistent with the two-sided dislocation. One-sided dislocations exhibit nonlinear frequency interaction giving quasi-periodic velocity fluctuations and spectra. A low beat frequency emerges (i.e. the dislocation frequency), whose energy grows downstream. It seems that these characteristics are almost ubiquitous features of one-sided dislocations, and the present work confirms similar phenomena for two-sided dislocations.

8.2. *Vortex dislocations in free shear flows*

The work by Browand & Troutt (1980, 1985) demonstrates that vortex 'defects' or dislocations are an essential feature of free shear layers, and could perhaps be the result of infinitesimal differences in flow uniformity across the span of a layer, as suggested by Browand & Ho (1987). Recent studies have been undertaken to force the appearance of dislocations in shear layers (Browand & Ho 1987; Browand & Prost-Domasky 1988; Browand *et al.* 1989; Nygaard & Glezer 1990). In the free shear layer, vortex branching is found, and the dislocations in some cases are also angled with respect to the free stream, as found for the wakes. It was further reported by Browand *et al.* (1989) that dislocations encourage the rapid appearance of low frequencies in the spectra as the flow travels downstream. This is caused in part by the tendency for the vortices neighbouring a dislocation to pair up locally (Yang

et al. 1990; Dallard & Browand 1991). Although this is somewhat different to the wake flows, where the pairing instability is far weaker, both flows exhibit the rapid growth of low frequencies due to dislocations. Nygaard & Glezer also show that dislocations in a shear layer produce strong streamwise vorticity in the flow, a fact which is clearly similar with the wake flow. There are therefore several characteristics of dislocations which are found similarly for wake and shear flows.

8.3. *Similarities of vortex dislocations with boundary-layer spots*

A great number of studies have been undertaken regarding the transition from laminar to turbulent flow in boundary layers, with many of them paying particular attention to the evolution of turbulent 'spots'. Such spots are described, for example, in the reviews of Coles (1981), Cantwell (1981), and Riley & Gad-el-Hak (1985). It seems that there are a number of similarities between vortex dislocations and turbulent spots, an immediate one being their appearance. In both cases they grow into an overall Λ-shaped structure. In the boundary layer, detailed measurements of the streamline pattern of an average spot by Coles & Barker (1975) and by Wygnanski *et al.* (1976) have shown that the ensemble-averaged spot is essentially a single large Λ-structure (known as a 'horseshoe vortex'), on which is superimposed smaller eddies. However, there is some debate regarding the overall structure of a turbulent spot, as outlined by Riley & Gad-el-Hak (1985).

There is also correspondence with the numerical values for the spreading angle of spots and dislocations. Schubauer & Klebanoff (1956) observed that turbulent spots, initiated by a spark technique, spread out spanwise with a half angle of close to 11°. Spots generated by Gad-el-Hak *et al.* using a roughness element and by Wygnanski *et al.* using the spark method give a half-angle near 10°. These values are remarkably close to the present visual spreading angle of two-sided dislocations, for which a value of around 12° is measured. Gad-el-Hak *et al.* also find that spanwise profiles of mean and fluctuating velocities in the region downstream of a roughness element yield broad maxima. Similar maxima are caused by vortex dislocations in the wake.

Gad-el-Hak *et al.* (1981) undertook an interesting experiment in which they heated their roughness element to observe the spanwise spread of its wake and found that it was significantly smaller than the overall size of the turbulent region. Similar results were obtained using two-colour flow visualization. They concluded that the spot grows laterally, not simply by entrainment, but from 'growth by destabilization' whereby the spot somehow destabilizes the otherwise laminar flow in its neighbourhood. In the present study, the two-colour visualizations of figures 19 and 20 show also that the lateral spreading of a dislocation occurs far more rapidly than the spread of the disturbance wake itself. Here, the spreading is by the outward axial flows in the vortices. It is not known whether the spanwise spreading in the wake dislocation and the boundary-layer spot are related, though it is conceivable.

Based on the existence of dislocations in wake and shear flow transition, one might suggest (in a speculative manner) a scenario for boundary layers involving dislocations as a trigger for turbulent spots, as shown in figure 33. It seems possible that slight spanwise non-uniformities in a boundary-layer flow could lead to a non-uniform development of Tollmien–Schlichting (TS) waves across the span, due in part to the relatively broad frequency receptivity. The interactions between neighbouring TS-wave 'cells' could form one-sided dislocations, which could grow rapidly spanwise, and result in the nucleus for turbulent spots. It is relevant to mention here some computations by Kim & Moin (1986) and by Choi & Guezennec (1990), which indicate that structures in channel flows and turbulent boundary layers are very often asymmetric or 'one-legged', which suggests that one should not

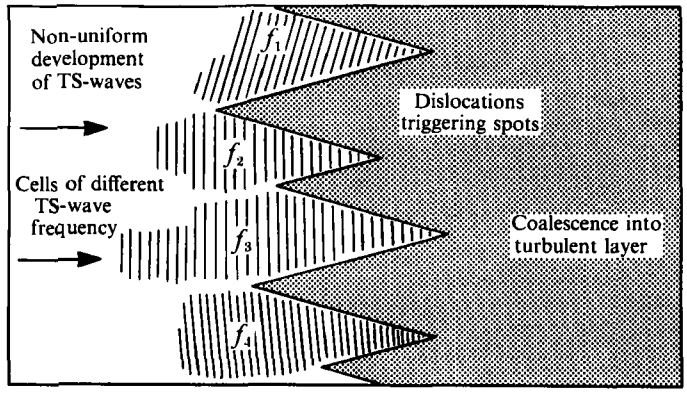

FIGURE 33. Scenario involving TS-wave dislocations as triggers for boundary-layer spots. This scenario for boundary-layer transition involves the non-uniform development of TS-waves across the span. This would lead to dislocation interactions between the different TS-wave cells, which would spread rapidly spanwise, and develop into spots of turbulence.

necessarily expect two-sided structures alone. As regards two-sided structures in a boundary layer, one can envisage slight local phase variations occurring in an otherwise constant-phase TS-cell, which would generate two-sided symmetric dislocations. The ideas above are only suggestive, and there are clearly significant differences between TS-waves and wake vortices, in particular their strengths. However, it seems, in analogy with the wake structures, that such a scenario described above is conceivable. If it is not simply observed in a natural boundary layer, such a scenario could possibly be induced by only small perturbations.

9. Three-dimensional transition in the cylinder wake: comparison of natural and forced vortex dislocations

A discussion of some aspects of three-dimensional transition was given in §4, followed by a detailed investigation of forced vortex dislocations. We are now in a position to compare some of the characteristics of natural transition with features of a wake where dislocations are forced.

Observations of dislocations in natural transition and in a wake with forced vortex dislocations seem remarkably similar, as can be seen in figure 34. In both cases, we can see the looping of vorticity in the central region, the streamwise bending of vortex filaments at the sides of the structure, and the nearly in-phase linking above and below the structures. One of the most significant similarities is the rapid spanwise spreading of both of these dislocations. There seems little doubt, from such visualizations, that the two structures are the same phenomenon with the same dynamic characteristics.

In order to clearly summarize the principal similarities between velocity measurements for natural and forced dislocations, several selected measurements are brought together in figure 35. The use of a point disturbance to trigger symmetric dislocations causes *periodic* dislocations, while the natural transition involves the appearance of *intermittent* dislocations. This is reflected by the velocity signals for each case in figure 35, where the intermittent dislocations cause the large irregular fluctuations, while the periodic dislocations cause large regular oscillations. Bloor (1964) had suggested, on the basis of work by Sato & Kuriki (1961), that the natural irregularities must be due to some form of three-dimensionality, and it now appears

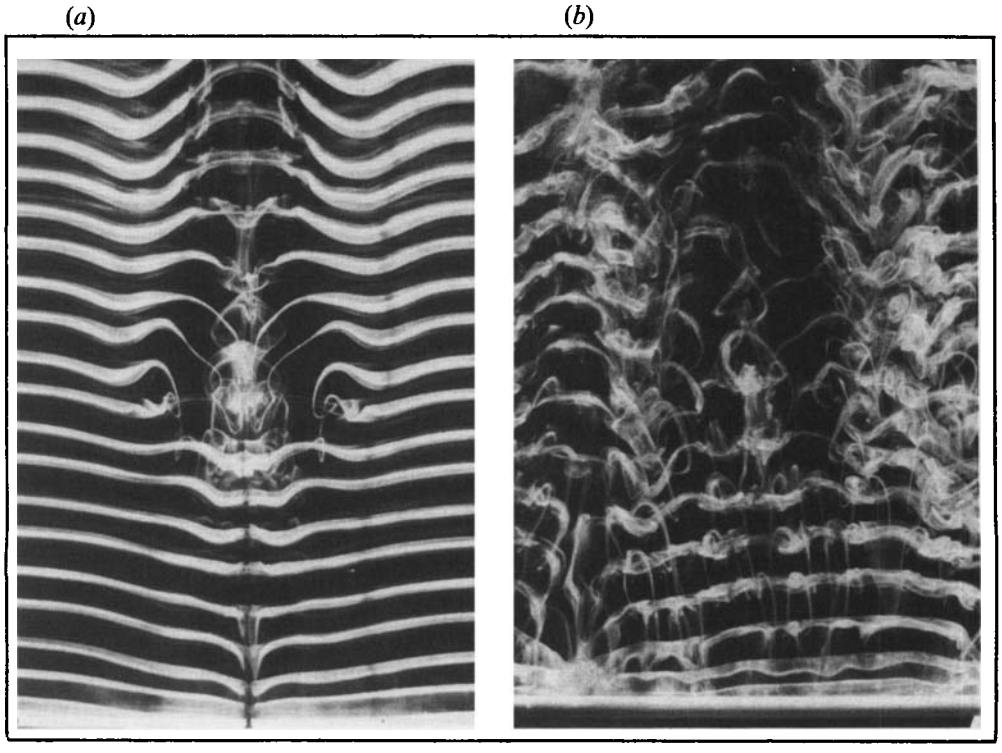

FIGURE 34. Similarities between forced and natural symmetric dislocations. There are close similarities between the forced (*a*) and natural symmetric dislocations (*b*), including the central looping of vortex tubes, the streamwise bending of vortices at the edges of the dislocation, and the overall shape and size of such dislocations. In both cases, the structures spread spanwise to form large-scale spot-like *A*-structures downstream.

that these irregularities are primarily due to dislocations. It is interesting to note that Sato (1970), who also compared natural transition to a two-frequency forcing case for the wake of a symmetric airfoil, found that the behaviour of the slow irregular fluctuation in the natural transition closely resembled that of the periodic low beat frequencies in the forced case. He suggested that these fluctuations were produced by the same mechanism. His suggestion is wholly in accordance with the present results.

There is also an obvious similarity in figure 35 between the transverse fluctuation profiles for natural transition and for forced dislocations, both of which show a maximum in the centre. This central maximum is caused by the *transverse symmetry* of the large-scale dislocations, which induce maximum fluctuations in the wake centreplane. At the bottom of figure 35, we may compare the decay of fluctuation levels as the wake progresses downstream. On the left, there is a rapid exponential decay of the integrated energy E for the laminar street wake as it travels downstream, whereas the energy for the wake with dislocations decays much more slowly. The same is true of the natural transition (on the right), where the decay of energy E is far slower for the transition case ($Re = 183$) than it is in the laminar case ($Re = 152$).

A comparison of velocity spectra in figure 36 shows that both the natural and forced dislocations produce a peak at low frequencies, which swamps the energy

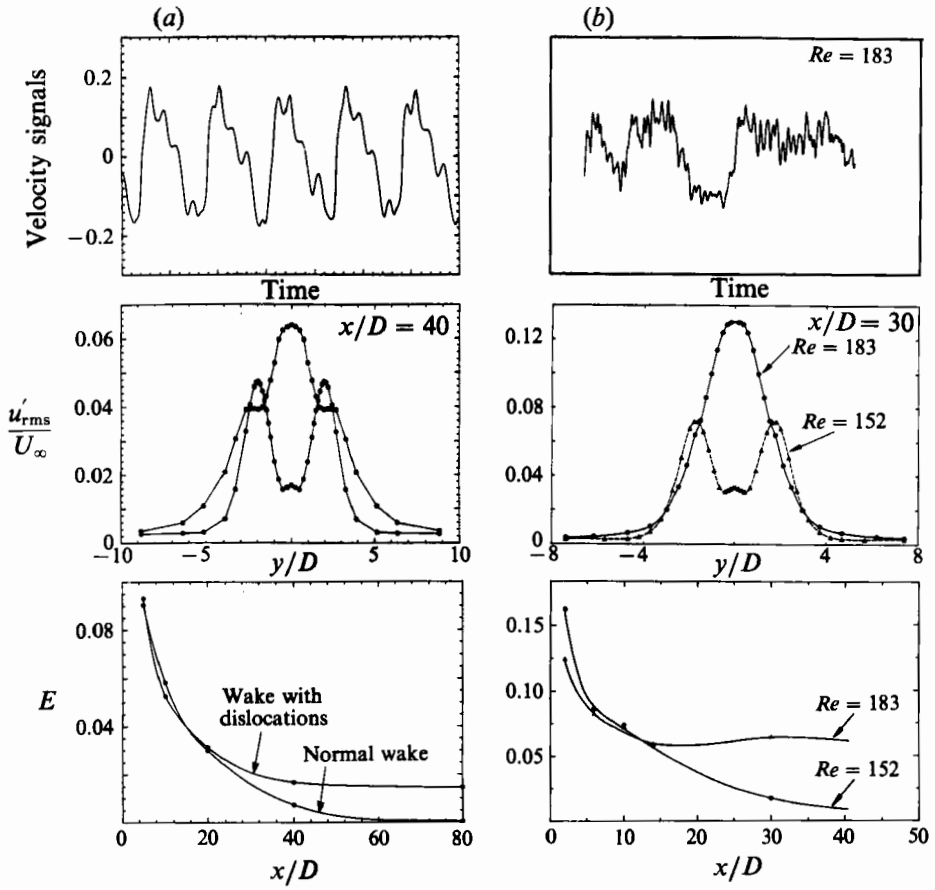

FIGURE 35. Comparison of natural and forced wake velocity measurements. Distinctly similar features are found for the forced dislocation (*a*) and for the natural dislocation (*b*). In both cases, there are large downstream velocity fluctuations (periodic in the forced case, and intermittent for the natural transition case). There are similarities in the fluctuation profiles and also the slow decay of energy and fluctuation level downstream.

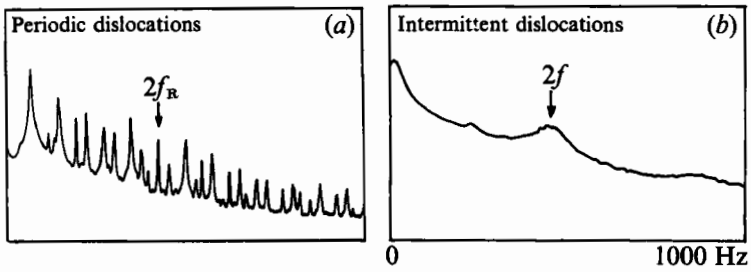

FIGURE 36. Comparison of forced and natural velocity spectra. In both (*a*) the forced and (*b*) natural dislocation cases, there is a large low-frequency peak in the energy, which swamps the energy at the original shedding frequencies (marked as f_R and f). These spectra are for (*a*) $x/D = 40$ and (*b*) $x/D = 30$.

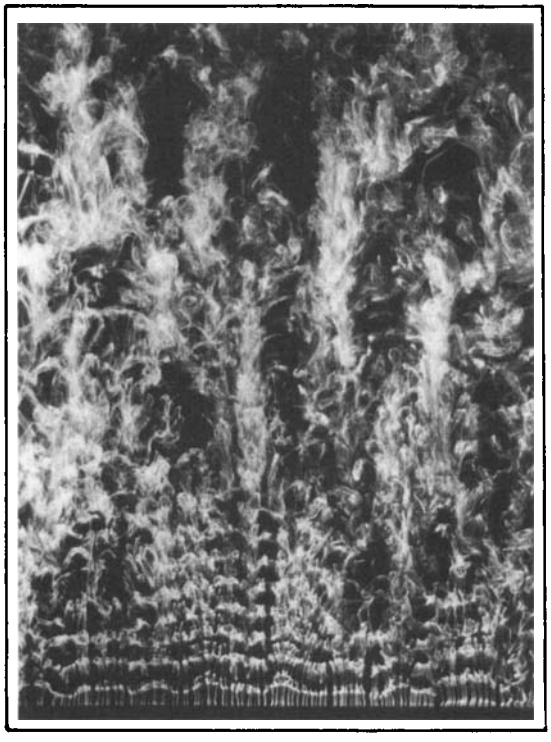

FIGURE 37. A 'cluster' of vortex dislocations occurring in natural transition. At this Reynolds number, there are roughly two dislocations appearing over a square area of $100\lambda^2$, which is comparable to the occurrence of dislocations found in a free shear layer by Browand & Prost-Domasky (1990). $Re = 200$. (The dislocations are evident as the distinct darker regions in the visualization.)

remaining from the upstream shed vortices at frequencies $2f$ and $2f_R$. The periodic forced dislocations exhibit quasi-periodicity, with a number of combination frequency peaks, the largest being at the low dislocation frequency. The intermittent natural dislocations induce a broad peak at low frequencies.

An example of smoke flow visualization from a wind tunnel in figure 37, shows a 'cluster' of dislocations in spanview, demonstrating that dislocations occur intermittently in space and time in a transitional wake. It should also be mentioned that work by Hama (1957), Gerrard (1978), Cimbala (1984) and Gerich (1987) all display examples of visualizations from which dislocations may be observed, although they were not recognized as such. Using figure 37, we may grasp some idea of the number of dislocations that will be found in a given centreplane area, which was similarly determined, using a rake of hot wires in a free shear flow, by Browand & Prost-Domasky (1990). They found that in a span of ten vortex wavelengths (λ), and during the time required for the passage of ten vortices, one to two vortex defects (dislocations) appeared on average. In the present visualization, we find, at this particular Reynolds number, approximately two dislocations per (square) area of $100\lambda^2$, which is of the same order as for the shear layer.

Finally, despite all of the above, it has not yet been proven that the 'glitches' or irregularities observed by Roshko (1954) in his figure 7 (*b*), and later by Bloor (1964), are definitely associated with the vortex dislocation structures in the wake. To resolve this question, it was decided to undertake an experiment involving simultaneous flow visualization and velocity measurements for a (transition) wake at

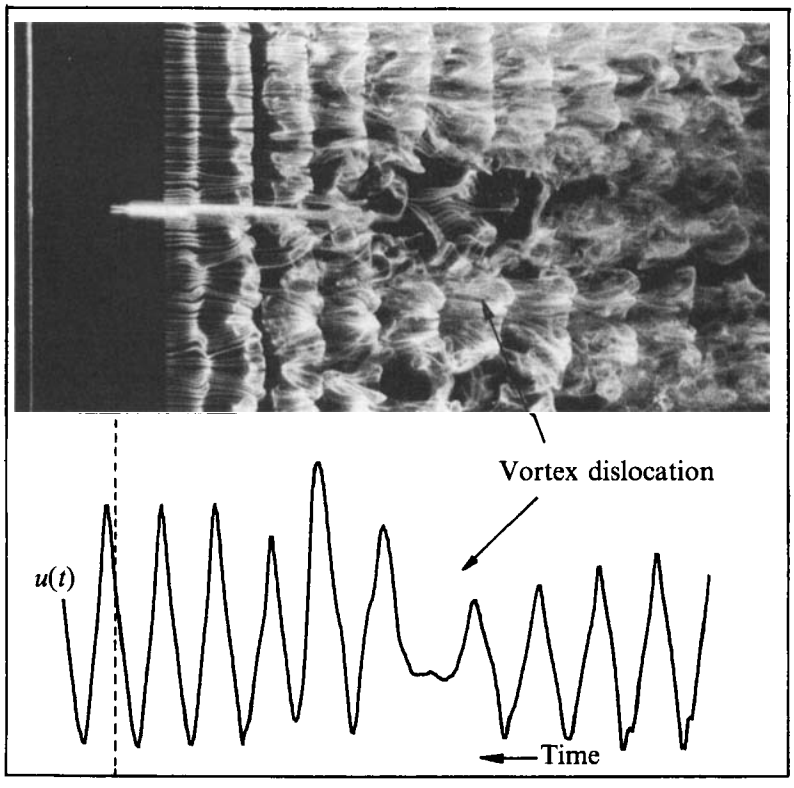

FIGURE 38. Simultaneous visualization of a dislocation with corresponding velocity measurements. This simultaneous visualisation using smoke in a wind tunnel (introduced into the flow at $x/D = 12$) with the corresponding velocity fluctuations shown below, proves that a glitch (or irregularity) found in the velocity signal does indeed correspond to a vortex dislocation structure in the flow. The photograph was taken at the time associated with the vertical dashed line. The hot wire supports are seen as the two small prongs to the left of the smoke wire.

$Re = 200$, in the wind tunnel. These results are shown in figure 38. (In this figure, it should be noted that, although the velocity signal has been shown 'to-scale' with the visualization above it, the measurements are only made at the position of the hot wire and do not represent developments in the wake as it travels downstream.) The conclusion to be drawn from figure 38 is that the irregularities or 'glitches' in the velocity signal directly correspond with the passage of dislocations past the hot wire.

On the basis of these results, one can summarize the characteristics of the transition to turbulence of the wake. Bloor (1964) concluded from her study that transition to turbulence occurs in two ways. (*a*) At lower Reynolds numbers, there is downstream distortion by (assumed) large-scale three-dimensionalities of vortices that are initially laminar within the vortex formation region. (*b*) At higher Reynolds numbers (above 1300), there is turbulence formed by the shear-layer instability within the vortex formation region. This instability is basically two-dimensional, but rapidly becomes three-dimensional, causing small-scale turbulent fluctuations. These latter results have been confirmed by Wei & Smith (1986) and by Braza, Chassaing & Ha Minh (1990). In the present work, the transition to turbulence is somewhat modified from the above. The downstream distortion appears on vortices that have already become three-dimensionally turbulent from within the vortex formation region. These downstream distortions are caused primarily (but not wholly) by

vortex dislocations. Therefore, one might summarize the transition to turbulence in the wake by including the following physical features, of all of which have their origin *within* the vortex formation region:

(*a*) Small-scale streamwise vortices appear within the vortex formation region (modes A and B), and are associated with primary vortex deformation in this region.

(*b*) Large-scale vortex dislocations (which are initiated within the vortex formation region) are primarily responsible for the large-scale distortions and break-up to turbulence downstream. A fundamental part of the distortion is due to axial core flows in the vortices as they travel downstream.

(*c*) Shear-layer instability vortices appear as the next stage in the transition to turbulence, at higher Reynolds numbers. This shear-layer transition causes fine-scale three-dimensional turbulence to be introduced within the vortex formation region.

Detailed measurements and visualizations for dislocations in natural transition are part of a further comprehensive paper concerning all aspects of the three-dimensional transition of the cylinder wake (Williamson 1992).

10. Conclusions

The transition to three-dimensionality and turbulence in a wake involves the appearance of certain fundamental physical phenomena, which are triggered by instabilities within the vortex formation region, and which may be summarized as follows:

(*a*) *Small-scale streamwise vortices* appear within the vortex formation region (at Reynolds numbers above 180), and are associated with primary vortex deformation in this region. Two modes of three-dimensional vortex shedding are denoted as mode A, involving vortex loops, and mode B, which is associated with finer-scale streamwise vortices. Each mode corresponds with a different frequency 'law', and with a different range of Reynolds numbers.

(*b*) *Large-scale vortex dislocations* are initiated within the vortex formation region (at Reynolds numbers above 180), due to phase variations caused by the slight randomness inherent in the three-dimensional modes of shedding, in the transition regime. These dislocations grow rapidly into large-scale structures as they travel downstream, and are responsible for much of the large-scale distortion and break-up to turbulence of the vortex wake.

(*c*) *Small-scale shear-layer instability vortices* are formed at higher Reynolds numbers (of around 1000), and are the next stage in the development of wake turbulence. This shear layer 'transition' causes the onset of further fine-scale three-dimensional turbulence within the vortex formation region (and has been studied elsewhere).

A principal discovery, in the present work, is that vortex dislocations are a fundamental characteristic of natural transition in a wake. Vortex dislocations are regions in the flow where the primary 'Kármán' vortices move out of phase with each other in the near wake, and thereafter grow into large-scale structures downstream. In natural transition their formation is intermittent in time and space, and their existence explains the large intermittent low-frequency velocity irregularities that were originally observed in the transition regime by Roshko (1954) and by Bloor (1964). The level of fluctuations in the transition wake is shown here to be much larger than in a laminar wake, with a much slower decay of fluctuation energy as the wake travels downstream.

In order to study the formation of dislocations in detail, they have been passively

forced or 'triggered' at a local spanwise position using a small ring disturbance around the cylinder. The marginally lower frequency of vortex shedding of the ring wake induces the vortices from the disturbance to dislocate with those to either side, forming a two-sided dislocation, as distinct from the one-sided dislocation that is found between (only) two cells of different frequency. The stable structure is shown to be a symmetric two-sided dislocation, where dislocations on each side of the ring form in phase with each other. Downstream, these structures grow into large A-shaped vortices which induce large periodic velocity fluctuations that are of similar magnitude to those found intermittently in natural transition. The quasi-periodic spectra of velocity fluctuations in the near wake are associated with a two-frequency interaction which, as the wake evolves downstream, gives way to spectra with almost all the energy lying at the (beat) dislocation frequency.

Visualization (including two-colour stereoscopy) demonstrates the main features of the vortex dynamics involved in a dislocation, in particular suggesting the type of vortex linking across a dislocation, the division or branching of vortices whereby a vortex may divide up and be connected to two other vortices of the same sign, and the mechanism for spanwise spreading of vortices at the edge of a dislocation. This spreading mechanism involves the helical twisting of vortex lines within a vortex, which thereby induces an axial core flow outwards from the dislocation. 'Fattened' cores sustain the outward flow by an axial pressure gradient, and leave behind them stretched vortex 'wisps' within the dislocation.

Distinct similarities are found between visualizations of vortex dislocations that occur naturally in transition and of those that are forced periodically. There are also marked similarities in the appearance of the downstream velocity signals (involving low-frequency fluctuations), in the shape of the fluctuation profiles and spectra, and in the slow rate of fluctuation energy decay, as the wake progresses downstream. Intrinsic to both natural transition and forced dislocations is the phenomenon of axial core flow and helical vortex twisting. It is suggested here that this axial flow, which leads to spanwise non-uniformities in the vortices, is a fundamental mechanism by which vortices develop large-scale distortions in natural transition.

Lastly, some of the features of dislocations that occur in the present case of *uniform* flow correspond with features of grossly *non-uniform* flows, such as the wake of a cone or stepped-cylinder, and for the sheared flow past a body. There are also similarities between dislocations in a wake and the 'defects' that are found naturally or forced in a free shear flow, and also between the wake A-structures and turbulent spots found in a boundary layer. A scenario is suggested whereby TS wave dislocations could go on to trigger turbulent spots in a transitioning boundary layer.

Similarities of dislocations between different types of flow suggest that vortex or phase dislocations could conceivably be a generic feature of transition in all shear flows.

The author would like to thank Kristen Gledhill at Cornell for her most efficient help in organizing many of the plots, including the colour contour plotting, and also to thank Anil Prasad for his enthusiastic help in arranging the smoke visualisations, and Greg Miller for assistance in the simultaneous visualization/velocity measurement study. Thanks are due to Dr Dean Taylor for allowing the use of his computers for the contour plotting. The author is also grateful to Ich Sugioka and Dr Jeff Jacobs who, in early 1988, were most encouraging when the symmetric dislocations were first observed, and to Dr Steve Schneider for discussion regarding dislocations in a boundary layer. The author thanks also Michael A. P. Gower for indispensable

assistance during the paper preparation. This work was supported at Cornell by an ONR Contract No. N00014-90-J-1686, as part of the 'Bluff Body Wake Vortex Dynamics' Accelerated Research Initiative. Some of the early work was conducted at Caltech under ONR Contract No. N00014-84-K-0618, of which the P.I. was Anatol Roshko, and to whom the author is indeed most grateful.

Appendix A. Effect of a variation of cylinder geometry and Reynolds number

A small investigation on the effects of varying the geometry of the ring disturbance was undertaken, as well as a study on the effects of Reynolds number on the formation of dislocations. It is found, from flow visualization and measurements, that the characteristics of vortex dislocations are basically similar under a wide range of conditions.

Over a range of Reynolds number, and for the ratio of ring diameter to cylinder diameter of 1.5 (i.e. $D_R/D = 1.5$), the relevant wake frequencies were measured, and are shown in figure 39(*a*). The dislocation Strouhal number (denoted S_D) is given by $S_D = S - S_R$, where S is the cylinder Strouhal number and S_R is the ring Strouhal number. All three Strouhal numbers are normalized by the cylinder diameter. It is interesting to note that the frequency of vortex shedding behind the ring (which has a spanwise length of only $\frac{1}{2}D$) is close to that which is predicted from a long cylinder (of order $100D$ and more) which has the same diameter and Reynolds number as the ring itself. This is felt to be fortuitous, but it suggests that one can rather roughly predict dislocation frequencies and wavelengths from the ratio D_R/D alone. A rough estimate of dislocation frequency can be given as

$$f_D/f = 1 - D_R/D,$$

and the wavelength of a dislocation (λ_D) as

$$\lambda_D/\lambda = (D_R/D)/(D_R/D - 1).$$

This trend of decreasing dislocation frequency with decreasing ring diameter is seen in the measured values of S_D in figure 39(*b*). One would also expect the wavelength to increase as D_R decreases, as is found in §6.

Finally, it is also found from flow visualization that the 'visual' spreading angle of the dislocations is reasonably unaffected by the dislocation frequency (or wavelength), or indeed by the spanlength of the ring disturbance. As regards the spanlength, one might not expect synchronization of the dislocations on each side of the ring if it is too long.

Appendix B. Instructions for stereoscopic viewing

In order to understand what one is trying to achieve by stereoscopy it is worth briefly describing its basis. When we look at an object, each eye sees a slightly different image. As we look with both eyes, the two different impressions on the retina are united into one single image in the brain. The sensation is one of viewing the object with a single eye, and the process is called *strereopsis*. Stereoscopy is used a great deal in chemistry and biology to display complex three-dimensional molecules, and it has also been used to view terrain on other planets (as used in the 'Viking Lander' mission), amongst many other applications. The usual display comprises two images of an object, each one being taken from a slightly different

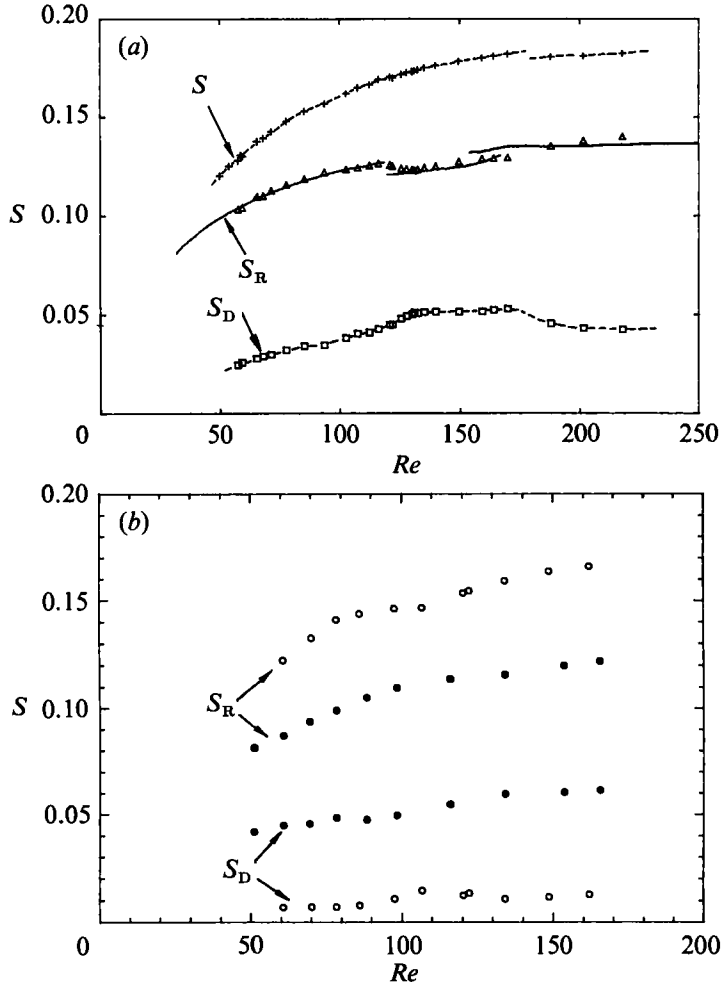

FIGURE 39. Effects of varying Reynolds number and D_R/D. In (*a*), the Strouhal numbers (S) versus Reynolds number (Re) for a vortex street are shown, along with the Strouhal number for the ring disturbance wake (S_R), and the resulting dislocation Strouhal number (S_D). In (*b*), the effect on S_R and S_D of a change in ring diameter D_R/D is shown: ○, $D_R = 1.2D$; ●, $D_R = 2.0D$.

angle relative to the object, roughly as each eye would see it. This is achieved in the present paper by the use of two side-by-side synchronized cameras. Although probably the best and simplest results can be communicated with a stereo slide viewer (and which has also been done in the present research), it is clearly not suited to publication in a journal. For the latter purpose, we have used pairs of photographs arranged side-by-side, with a separation between equivalent points in each picture of around 6.5 cm. This is the average distance between a pair of adult human eyes.

One method to enable each eye to see a separate image is to use a standard stereo viewer (comprising a pair of lenses, each of which is mounted directly above one of the images) which can be readily purchased from scientific laboratory suppliers, and elsewhere. Another method is called 'free-viewing', involving basically two different techniques. The first technique with 'parallel view lines' may be used (where the right eye sees the right image and the left eye sees the left image), although this is rather difficult for the observer to accomplish. A more usual technique is to use

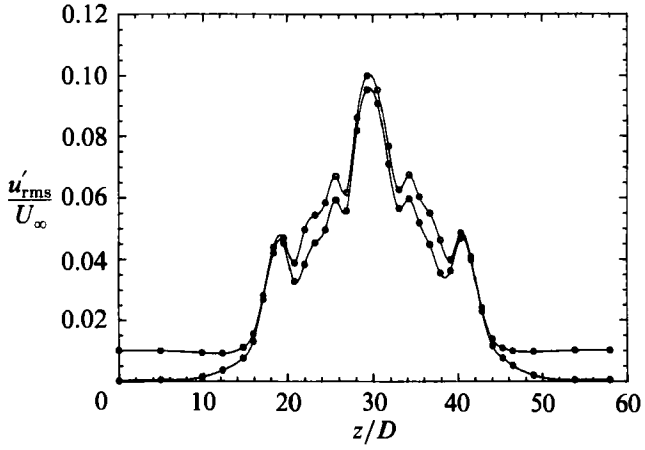

FIGURE 40. Ensemble-averaged fluctuation profiles. This plot shows that if all the harmonics of f_D are taken into account (by ensemble averaging at frequency f_D), then almost all the total fluctuation energy is accounted for. $x/D = 40$, $y/D = 0$. ○, $(u'_{rms}/U_\infty)_{total}$; ●, $\langle u'_{rms}/U_\infty \rangle_{f_D}$.

'transverse view lines', where the observer sees each image more or less 'cross-eyed'. Our left eye looks at the right image, and vice versa. In this method, one will see three images next to each other, and we should pay attention to the central 'stereoscopic' one, which should be the same size as the real side images. One should concentrate on features within the image, and patiently give the brain time to adjust. It will be very clear when stereoscopy is achieved, and if there is some doubt at all, then it is likely that the viewing is not correct. For this 'cross-eyed' technique, it is very important to have strong lighting on the photographs. One should also view the pairs of images from a distance of the order of 6–12 in. away (or more). Once the three-dimensionality is well observed, it will be clear how much information is otherwise lost in two dimensions.

Appendix C. Ensemble-averaged measurements

Ensemble-averaged measurements were made in §7, where velocity signals (from one hot wire) across the span, at $x/D = 40$, were referenced to a second fixed hot wire. By these means an 'instantaneous' picture of the velocities in a complete dislocation structure can be estimated. Using the same data, we can also calculate the value of (u'_{rms}/U_∞) corresponding *only* with the dislocation frequency f_D (and all of its harmonics). The result, shown in figure 40, demonstrates that practically all of the energy associated with dislocations at $x/D = 40$ is due to the dislocation waveform alone.

REFERENCES

ALBAREDE, P. 1991 Self-organisation in the three-dimensional wakes of bluff bodies. Thése de Doctorat de l'Universite de Provence, France.

ALBAREDE, P. & MONKEWITZ, P. 1992 A model for the formation of oblique shedding patterns and 'chevrons' in cylinder wakes. *Phys. Fluids* **A4**, 744.

ALBAREDE, P., PROVANSAL, M. & BOYER, L. 1990 Modelisation par l'equation de Guinzburg-Landau du sillage tri-dimensionel d'un obstacle allonge. *C. R. Acad. Sci. Paris* **310**, Serie II, 459.

BEARMAN, P. W. & SZEWCZYK, A. 1991 Effects of 3-D imposed disturbances on bluff body near wake flows. Presentation at *ONR Workshop on Bluff Body Wake Dynamics, Arizona State University, Tempe, Arizona.*

BERNAL, L. P. & ROSHKO, A. 1986 Streamwise vortex structure in plane mixing layers. *J. Fluid Mech.* **170**, 499.

BLOOR, M. S. 1964 The transition to turbulence in the wake of a circular cylinder. *J. Fluid Mech.* **19**, 290.

BROWAND, F. K. & HO, C.-M. 1987 Forced unbounded shear flows. *Nucl. Phys.* B (*Proc. Suppl.*) **2**, 139.

BROWAND, F. K., LEGENDRE, S. & TANIGUCHI, P. 1989 A model of vortex pairing induced by defects in mixing layers. *Bull. Am. Phys. Soc.* **34**, 2269.

BROWAND, F. K. & PROST-DOMASKY, S. A. 1988 Technique for acoustic excitation of separated shear flows: preliminary results. *ASME Winter meeting, Chicago, Illinois.*

BROWAND, F. K. & PROST-DOMASKY, S. A. 1990 Experiment on pattern evolution in the 2-D mixing layer. In *New Trends in Nonlinear Dynamics and Pattern Forming Phenomena* (ed. P. Coullet & P. Huerre), p. 159. NATO ASI Series 8. Plenum.

BROWAND, F. K. & TROUTT, T. R. 1980 A note on the spanwise structure in the two-dimensional mixing layer. *J. Fluid Mech.* **97**, 771.

BROWAND, F. K. & TROUTT, T. R. 1985 The turbulent mixing layer: geometry of large vortices. *J. Fluid Mech.* **158**, 489.

CANTWELL, B. 1981 Organised motion in turbulent flow. *Ann. Rev. Fluid Mech.* **13**, 457.

CANTWELL, B., COLES, D. & DIMOTAKIS P. 1978 Structure and entrainment in the plane of symmetry of a turbulent spot. *J. Fluid Mech.* **87**, 641.

CHOI, W. C. & GUEZENNEC, Y. G. 1990 On the asymmetry of structures in turbulent boundary layers. *Phys. Fluids* A **2**, 628.

CIMBALA, J. M. 1984 Large structure in the far wakes of two-dimensional bluff bodies. Ph.D. thesis, Graduate Aeronautical Laboratories, California Institute of Technology.

CIMBALA, J. M., NAGIB, H. M. & ROSHKO, A. 1988 Large structure in the far wakes of two-dimensional bluff bodies. *J. Fluid Mech.* **190**, 265.

COLES, D. 1981 Prospects for useful research on coherent structure in turbulent shear flow. *Proc. Indian Acad. Sci: Eng. Sci.* **4**, 111.

COLES, D. & BARKER, S. J. 1975 Some remarks on a synthetic turbulent boundary layer. In *Turbulent Mixing in Non-reactive and Reactive Flows* (ed. S. N. B. Murphy), p. 285. Plenum.

DALLARD, T. & BROWAND, F. K. 1991 Scale transitions at defect sites in the mixing layer: application of the 2-D arc wavelet transform. *J. Fluid Mech.* (submitted).

EISENLOHR, H. 1986 Investigations of the wake of a plate parallel to the flow with a blunt trailing edge. Diplom. thesis, Berich 3/1986, Max-Planck-Inst fur Stromungsforschung, Gottingen (In German).

EISENLOHR, H. & ECKELMANN, H. 1989 Vortex splitting and its consequences in the vortex street wake of cylinders at low Reynolds number. *Phys. Fluids* A **1**, 189.

GAD-EL-HAK, M., BLACKWELDER, R. F. & RILEY, J. J. 1981 On the growth of turbulent regions in laminar boundary layers. *J. Fluid Mech.* **110**, 73.

GASTER, M. 1969 Vortex shedding from slender cones at low Reynolds numbers. *J. Fluid Mech.* **38**, 565.

GASTER, M. 1971 Vortex shedding from circular cylinders at low Reynolds numbers. *J. Fluid Mech.* **46**, 749.

GERICH, D. 1986 Uber die Veranderung der Karmanschen Wirbelstrasse durch Endscheiben an einem Kreiszylinder. Ph.D. thesis, Mitteilungen Nr. 81, Max Planck Institut fur Stromungsforschung, Gottingen.

GERICH, D. 1987 Uber den kontinuierlich arbeitenden Rauchdraht und die Sichtbarmachung eines Ubergangs vom laminaren zum turbulenten Nachlauf. *Bericht* 104/1987. Max Planck Institut fur Stromungsforschung, Gottingen.

GERICH, D. & ECKELMANN, H. 1982 Influence of end plates and free ends on the shedding frequency of circular cylinders. *J. Fluid Mech.* **122**, 109.

GERRARD, J. H. 1978 The wakes of cylindrical bluff bodies at low Reynolds number. *Phil. Trans. R. Soc. Lond.* A **288**, 351.

GRIFFIN, O. M. 1988 The effects of current shear on vortex shedding. *Marine Technology Div. Rep.* Naval Research Laboratory.

HAMA, F. R. 1957 Three-dimensional vortex pattern behind a circular cylinder. *J. Aeronaut. Sci.* **24**, 156.

JESPERSON, D. C. & LEVIT, D. 1991 Numerical simulation of flow past a tapered cylinder. *29th Aerospace Sciences Meeting, Reno, Nevada, AIAA Paper* 91-0751.

KIM, J. & MOIN. 1986 The structure of the vorticity field in turbulent channel flow. Part 2. Study of ensemble-averaged fields. *J. Fluid Mech.* **162**, 339.

KONIG, M., EISENLOHR, H., ECKELMANN, H. 1990 The fine structure in the *S–Re* relationship of the laminar wake of a circular cylinder. *Phys. Fluids* A **2**, 1607.

LEONARD, A. 1985 Computing three-dimensional incompressible flows with vortex elements. *Ann. Rev Fluid Mech.* **17**, 523.

LEWIS, C. & GHARIB, M. 1992 An exploration of the wake three-dimensionalities caused by a local discontinuity in cylinder diameter. *Phys. Fluids* A **4**, 104.

LUNDGREN, T. S. & ASHURST, W. T. 1989 Area-varying waves on curved vortex tubes with application to vortex breakdown. *J. Fluid Mech.* **200**, 283.

MAULL, D. J. & YOUNG, R. A. 1973 Vortex shedding from bluff bodies in a shear flow. *J. Fluid Mech.* **60**, 401.

MEIBURG, E. & LASHERAS, J. 1988 Experimental and numerical investigation of the three-dimensional transition in plane wakes. *J. Fluid Mech.* **190**, 1.

MONKEWITZ, P., ALBAREDE, P. & CLAVIN, P. 1990 A simple theoretical model for the formation of 'chevrons' in the wake of a cylinder. *Bull. Am. Phys. Soc.* **35**, 2320.

NOACK, B. N., OHLE, F. & ECKELMANN, H. 1991 On cell formation in vortex streets. *J. Fluid Mech.* **227**, 293.

NYGAARD, K. J. & GLEZER, A. 1990 Core instability of the spanwise vortices in a plane mixing layer. *Phys. Fluids* A **2**, 461.

PARK, D. S. & REDEKOPP, L. G. 1991 A model for pattern selection in wake flows. *Phys. Fluids* (submitted).

PERRY, A. E. & CHONG, M. S. 1982 On the mechanism of wall turbulence. *J. Fluid Mech.* **119**, 173.

PICIRILLO, P. S. & VAN ATTA, C. W. 1991 An experimental study of vortex shedding behind a linearly tapered cylinder at low Reynolds number. *J. Fluid Mech.* (submitted).

RILEY, J. J. & GAD-EL-HAK, M. 1985 The dynamics of turbulent spots. In *Frontiers in Fluid Mechanics* (ed. S. H. Davis and J. L. Lumley), p. 123. Springer.

ROCKWELL, D., NUZZI, F. & MAGNESS, C. 1991 Period doubling in the wake of a three-dimensional cylinder. *Phys. Fluids* A **3**, 1477.

ROSHKO, A. 1954 On the development of turbulent wakes from vortex streets. *NACA Rep.* 1191.

SATO, H. 1970 An experimental study of non-linear interaction of velocity fluctuations in the transition region of a two-dimensional wake. *J. Fluid Mech.* **44**, 741.

SATO, H. & KURIKI, K. 1961 The mechanism of transition in the wake of a thin flat plate placed parallel to a uniform flow. *J. Fluid Mech.* **11**, 321.

SCHUBAUER, G. B. & KLEBANOFF, P. S. 1956 Contributions on the mechanics of boundary layer transition. *NACA Rep.* 1289.

SLAOUTI, A. & GERRARD, J. H. 1981 An experimental investigation of the end effects on the wake of a circular cylinder towed through water at low Reynolds numbers. *J. Fluid Mech.* **112**, 297.

VAN ATTA, C., GHARIB, M. & HAMMACHE, M. 1988 Three-dimensional structure of ordered and chaotic vortex streets behind circular cylinders at low Reynolds Numbers. *Fluid Dyn. Res.* **3**, 127.

WEI, T. & SMITH, C. R. 1986 Secondary vortices in the wake of circular cylinders. *J. Fluid Mech.* **169**, 513.

WILLIAMSON, C. H. K. 1988*a* Defining a universal and continuous Strouhal–Reynolds number relationship for the laminar vortex shedding of a circular cylinder. *Phys. Fluids* **31**, 2742.

WILLIAMSON, C. H. K. 1988*b* The existence of two stages in the transition to three-dimensionality of a cylinder wake. *Phys. Fluids* **31**, 3165.

WILLIAMSON, C. H. K. 1989*a* Oblique and parallel modes of vortex shedding in the wake of a circular cylinder at low Reynolds numbers. *J. Fluid Mech.* **206**, 579.

WILLIAMSON, C. H. K. 1989*b* Generation of periodic vortex dislocations due to a point disturbance in a planar wake, *Phys. Fluids* A **1**, 1444.

WILLIAMSON, C. H. K. 1991*a* 2-D and 3-D aspects of the wake of a cylinder, and their relation to wake computations. In *Proc. Conf. on Vortex Dynamics and Vortex Methods.* AMS-SIAM Lectures in Applied Mathematics, vol. 28, p. 719.

WILLIAMSON, C. H. K. 1991*b* Three-dimensional aspects and transition in the wake of a cylinder. In *Turbulent Shear Flows 7* (ed. F. Durst & J. Launder), p. 173 Springer.

WILLIAMSON, C. H. K. 1991*c* The formation of spot-like A-structures caused by vortex dislocations in a wake. In *Proc. 8th Symp. on Turbulent Shear Flows, Technische Universitat, Munich, Germany, September 1991.*

WILLIAMSON, C. H. K. 1992 The transition to three-dimensionality in the wake of cylinders, *J. Fluid Mech.* (submitted).

WILLIAMS-STUBER, K. & GHARIB, M. 1990 Transition from order to chaos in the wake of an airfoil. *J. Fluid Mech.* **213**, 29.

WYGNANSKI, I., SOKOLOV, M. & FRIEDMAN, D. 1976 On a turbulent 'spot' in a laminar boundary layer. *J. Fluid Mech.* **78**, 785.

YANG, R. 1990 Two-dimensional models of pattern formation in free shear flows. Ph.D. thesis, Aerospace Department, University of Southern California.

YANG, R., HUERRE, P. & COULLET, P. 1990 A 2-D model of pattern evolution in mixing layers. In *New Trends in Nonlinear Dynamics and Pattern Phenomena*, (ed. P. Coullet & P. Huerre), p. 171. NATO ASI Series 8, Plenum.